Heating (Gapless) Color-Flavor Locked Quark Matter

Kenji Fukushima,[1,2] Chris Kouvaris,[1] and Krishna Rajagopal[1]

[1] *Center for Theoretical Physics, Massachusetts Institute of Technology, Cambridge, MA 02139, USA*
[2] *Department of Physics, University of Tokyo, 7-3-1 Hongo, Tokyo 113-0033, Japan*

(Dated: August 25, 2004)

We explore the phase diagram of neutral quark matter at high baryon density as a function of the temperature T and the strange quark mass M_s. At $T = 0$, there is a sharp distinction between the insulating color-flavor locked (CFL) phase, which occurs where $M_s^2/\mu < 2\Delta$, and the metallic gapless CFL phase, which occurs at larger M_s^2/μ. Here, μ is the chemical potential for quark number and Δ is the gap in the CFL phase. We find this distinction blurred at $T \neq 0$, as the CFL phase undergoes an insulator-to-metal crossover when it is heated. We present an analytic treatment of this crossover. At higher temperatures, we map out the phase transition lines at which the gap parameters Δ_1, Δ_2 and Δ_3 describing ds-pairing, us-pairing and ud-pairing respectively, go to zero in an NJL model. For small values of M_s^2/μ, we find that Δ_2 vanishes first, then Δ_1, then Δ_3. We find agreement with a previous Ginzburg-Landau analysis of the form of these transitions and find quantitative agreement with results obtained in full QCD at asymptotic density for ratios of coefficients in the Ginzburg-Landau potential. At larger M_s^2/μ, we find that Δ_1 vanishes first, then Δ_2, then Δ_3. Hence, we find a "doubly critical" point in the $(M_s^2/\mu, T)$-plane at which two lines of second order phase transitions ($\Delta_1 \to 0$ and $\Delta_2 \to 0$) cross. Because we do not make any small-M_s approximation, if we choose a relatively strong coupling leading to large gap parameters, we are able to pursue the analysis of the phase diagram all the way up to such large values of M_s that there are no strange quarks present.

PACS numbers: 12.38.-t, 25.75.Nq

I. INTRODUCTION

Our understanding of the properties of matter at high baryon number density has developed rapidly in the last several years. At any densities that are high enough that nucleons are crushed into quark matter, the quark matter that results must, at sufficiently low temperatures, be in one of a family of color superconducting phases [1]. The essence of color superconductivity is quark pairing, driven by the BCS mechanism which operates whenever there is an attractive interaction between fermions at a Fermi surface. The QCD quark-quark interaction is strong and is attractive between quarks that are antisymmetric in color, so we expect cold dense quark matter to generically exhibit color superconductivity. Color superconducting quark matter may well occur in the cores of compact stars.

It is by now well-established that at asymptotic densities, where the up, down and strange quarks can be treated on an equal footing and the disruptive effects of the strange quark mass can be neglected, quark matter is in the color-flavor locked (CFL) phase, in which quarks of all three colors and all three flavors form Cooper pairs [2]. The CFL phase is a color superconductor but is an electromagnetic insulator, with zero electron density.

To describe quark matter as may exist in the cores of compact stars, we need consider quark chemical potentials μ of order 500 MeV at most, meaning that the strange quark mass M_s must be included: it is expected to be density dependent, lying between the current mass ~ 100 MeV and the vacuum constituent quark mass ~ 500 MeV. In bulk matter, as is relevant for compact stars where we are interested in kilometer-scale volumes, we must furthermore require electromagnetic and color neutrality [3, 4] (possibly via mixing of oppositely charged phases) and allow for equilibration under the weak interactions. All these factors work to pull apart the Fermi momenta of the cross-species pairing that characterizes color-flavor locking. At the highest densities, we expect CFL pairing, but as the density decreases the combination of nonzero M_s and the constraints of neutrality put greater and greater stress on cross-species pairing, and reduce the excitation energies of those fermionic quasiparticles whose excitation would serve to ease the stress by breaking pairs [5].

If we imagine beginning in the CFL phase at asymptotic density, reducing the density, and assume that CFL pairing is disrupted by the heaviness of the strange quark before color superconducting quark matter is superseded by the hadronic phase, the next phase down in density is the gapless CFL phase [5, 6]. In this phase, quarks of all three colors and all three flavors still form Cooper pairs, but there are regions of momentum space in which certain quarks do not succeed in pairing, and these regions are bounded by momenta at which certain fermionic quasiparticles are gapless. The material is an electromagnetic conductor, with a nonzero electron density.

Our goal in this paper is to map the phase diagram of neutral dense quark matter at nonzero temperature, answering the question of what phases and phase transitions result when CFL or gCFL quark matter is heated. In the case of CFL quark matter with strange quark mass $M_s = 0$, this question has been answered in Ref. [7]. In this most symmetric setting, there is a single phase transition at a temperature $T_c^{\rm CFL}$ below which there is CFL

pairing and above which there is no pairing. In mean field theory,

$$T_c^{\rm CFL} = 2^{\frac{1}{3}} \frac{e^\gamma}{\pi} \Delta_0 \ , \qquad (1)$$

where Δ_0 is the CFL gap parameter at $T = 0$, estimated to be of order 10 to 100 MeV [1]. The enhancement of T_c/Δ_0 by a factor of $2^{1/3}$ over the standard BCS value (which our results confirm) originates in the fact that in the CFL phase with $M_s = 0$ there are eight fermionic quasiparticles with gap Δ_0 and one with gap $2\Delta_0$ [7]. As at any phase transition at which a superconducting order parameter melts, gauge field fluctuations that are neglected in mean field theory can elevate T_c and render the transition first order [8]. Because the gauge coupling in QCD is strong, these effects are significant [9, 10]. They have been evaluated to date only at $M_s = 0$ [9, 10]. Once $M_s \neq 0$, the mean field analysis alone becomes rather involved and we shall therefore leave the inclusion of fluctuations to future work.

To see why $M_s \neq 0$ results in an intricate phase diagram at nonzero temperature, we must introduce the pairing ansatz that we shall use throughout this paper [2, 5, 6, 11]:

$$\langle \psi_a^\alpha C\gamma_5 \psi_b^\beta \rangle \sim \Delta_1 \epsilon^{\alpha\beta 1}\epsilon_{ab1} + \Delta_2 \epsilon^{\alpha\beta 2}\epsilon_{ab2} + \Delta_3 \epsilon^{\alpha\beta 3}\epsilon_{ab3} \quad (2)$$

Here ψ_a^α is a quark of color $\alpha = (r, g, b)$ and flavor $a = (u, d, s)$; the condensate is a Lorentz scalar, antisymmetric in Dirac indices, antisymmetric in color (the channel with the strongest attraction between quarks), and consequently antisymmetric in flavor. The gap parameters Δ_1, Δ_2 and Δ_3 describe down-strange, up-strange and up-down Cooper pairs, respectively. At $T = 0$, there is an insulator-metal transition at $M_s^2/\mu \simeq 2\Delta_1$, at which the CFL insulator with $\Delta_3 \simeq \Delta_2 = \Delta_1$ is replaced by the gapless CFL metal, which has $\Delta_3 > \Delta_2 > \Delta_1 > 0$ [5, 6]. (If the CFL phase is augmented by a K^0-condensate [12], the CFL→gCFL transition is delayed to $M_s^2/\mu \simeq 8\Delta_1/3$ [13].) An analogous zero temperature metal insulator transition has been analyzed in Ref. [14].

At $M_s = 0$, $\Delta_1 = \Delta_2 = \Delta_3 = \Delta_{\rm CFL}$, and $\Delta_{\rm CFL}$ decreases from Δ_0 at $T = 0$ to 0 at $T_c^{\rm CFL}$. As soon as $M_s \neq 0$, however, we can expect that Δ_1, Δ_2 and Δ_3 do not all vanish at the same temperature. This expectation is evident for the gCFL phase, which has $\Delta_3 > \Delta_2 > \Delta_1 > 0$ already at $T = 0$. We shall see that it also applies to the CFL phase with $M_s \neq 0$.

The distinction between an insulator and a metal is sharp only at $T = 0$. At any nonzero temperature, there will be some nonzero density of thermally excited fermionic quasiparticles, some of which are charged. This means that the CFL→gCFL "transition" should be a crossover at any nonzero temperature [15]. The CFL phase at $T = 0$ with $M_s \neq 0$ has fermionic quasiparticles with opposite charges whose excitation energies differ. This means that upon heating this phase, the chemical potentials needed to maintain neutrality are not the same as at zero temperature. Adjusting the chemical potentials feeds back into the gap equations for Δ_1, Δ_2 and Δ_3 differently, and these gap parameters can therefore have different T-dependence. If we start in the CFL phase at $T = 0$, heat, then increase M_s^2/μ above that for the zero temperature CFL→gCFL transition, and then cool back to $T = 0$ we can go from CFL to gCFL without ever crossing a phase boundary. We illustrate this by showing an example phase diagram in Fig. 1.

The purpose of this paper is to derive and understand the phase diagram of Fig. 1. We shall present the model and approximations that we use in Section II. We follow the conventions for naming phases used in previous literature:

$\Delta_1, \Delta_2, \Delta_3 \neq 0$	(g)CFL
$\Delta_1 = 0, \quad \Delta_2, \Delta_3 \neq 0$	uSC
$\Delta_2 = 0, \quad \Delta_1, \Delta_3 \neq 0$	dSC
$\Delta_1 = \Delta_2 = 0, \quad \Delta_3 \neq 0$	(g)2SC
$\Delta_1 = \Delta_2 = \Delta_3 = 0$	UQM,

with "UQM" meaning unpaired quark matter. The origin of the remaining names is that in the 2SC phase, only quarks of two flavors and two colors pair, whereas in the uSC (or dSC) phase, all u (or all d) quarks pair [16]. The phase diagram features three lines denoting second order phase transitions at which Δ_1, Δ_2 or Δ_3 vanish. At $M_s = 0$, all three gaps vanish at the same temperature but at generic values of M_s, there are three distinct transition temperatures. Two of these lines cross at a point denoted by the circle: at this "doubly critical point", Δ_1 and Δ_2 vanish at the same temperature. The phase diagram is intricate, and one natural question is to what extent its features are generic. We address this by varying parameters, as we shall discuss in Sections III and IV. We shall find that the physics at large M_s^2/μ, where we find a first order phase transition in Fig. 1, is not generic, changing qualitatively for larger values of Δ_0. We find that the shape of the second order phase boundaries separating the CFL, dSC, uSC and 2SC phases is generic, as is the existence of the doubly critical point.

Physics in the vicinity of any of these phase transitions can be analyzed using a Ginzburg-Landau approximation, in which the relevant Δ or Δ's are taken to be small. This analysis has been performed at $M_s = 0$ in Refs. [3, 9, 17] and at small but nonzero M_s in Ref. [16]. We shall show in Section VI that our numerical results for the three phase transition lines at small $M_s^2/\mu\Delta_0$ are in quantitative agreement with the Ginzburg-Landau approximation, and shall show that the ratios of coefficients in the Ginzburg-Landau potential that we obtain in our model agree quite well with those obtained in full QCD at higher densities. At small $M_s^2/\mu\Delta_0$, the region of the phase diagram where the Ginzburg-Landau analysis applies near T_c, Δ_2 vanishes at a lower critical temperature than Δ_1. In heating gCFL quark matter, however, we expect Δ_1 to vanish first because it is already much smaller at $T = 0$. Our model analysis can be extended to larger

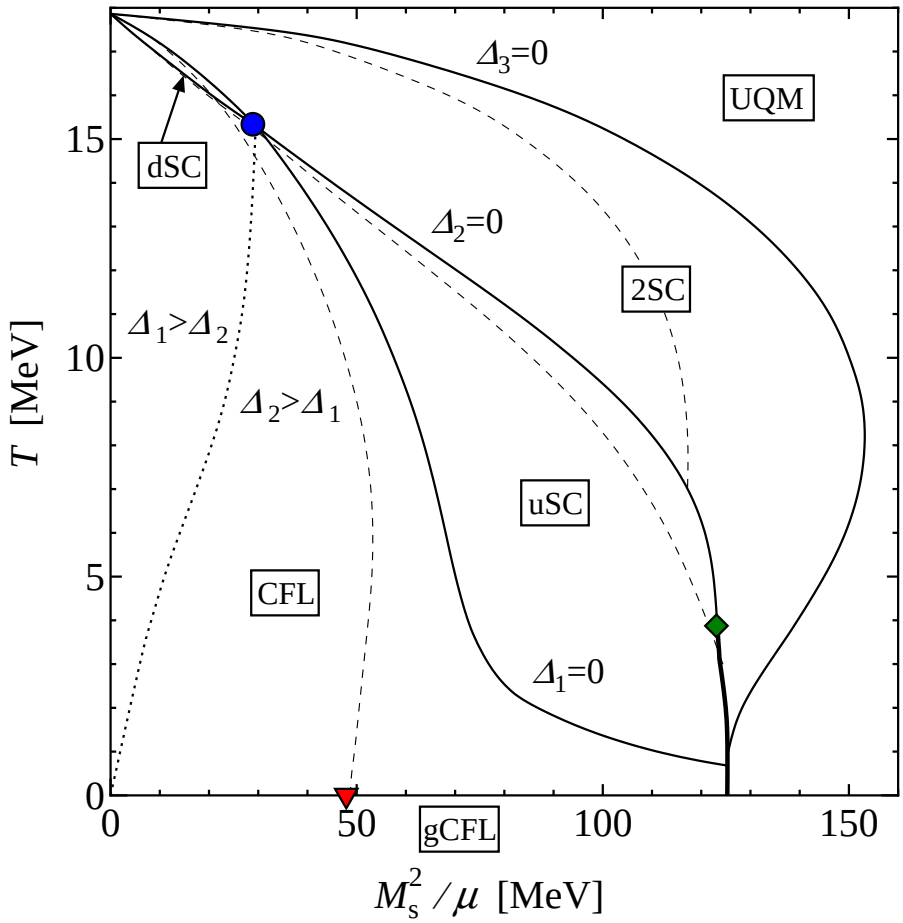

FIG. 1: Phase diagram of dense neutral quark matter in the $(M_s^2/\mu, T)$ plane. Only the solid curves represent phase transitions. The thin solid curves denote mean field second order phase transitions at which Δ_1 or Δ_2 or Δ_3 vanish. Two of these lines cross at the circle, which we call a "doubly critical" point. The heavy solid line is a first order phase transition that ends at a tricritical point denoted by the diamond. The dashed curves indicate locations where, as M_s^2/μ is increased, new gapless modes appear. At any nonzero temperature, however, there is no physical distinction between a phase with truly gapless modes and one in which the same modes have excitation energies of order T. The dashed curves therefore have physical significance only where they cross $T = 0$. In this phase diagram, this occurs only at the triangle, which denotes the zero temperature CFL→gCFL transition, which is a quantum critical point. The dotted line separates the $\Delta_1 > \Delta_2$ and $\Delta_2 > \Delta_1$ regions. This phase diagram is drawn for $\mu = 500$ MeV, with M_s and T varying, and with the quark-quark interaction strength fixed and chosen such that the CFL gap is $\Delta_0 = 25$ MeV at $T = 0$. We shall describe the model and approximations within which this phase diagram has been obtained in Section II, and describe the results summarized by this diagram in Sections III and IV.

M_s and smaller T than the Ginzburg-Landau analysis, allowing us to see how the phase diagram fits together, consistent with this expectation.

A phase diagram similar to ours was obtained previously in Ref. [15], but our results differ in a crucial, qualitative respect at low M_s^2/μ, where we believe that our results are robust: the authors of Ref. [15] found that Δ_1 always vanishes at a lower temperature than Δ_2, meaning that there is no dSC region on their phase diagram. This also disagrees with the Ginzburg-Landau analysis [47]. We shall detail our approximations in Section II, but we note already here that whereas in Refs. [5, 6, 15] M_s was assumed to be much smaller than μ, we do not make such an approximation. This likely explains the differences between our results and those of Ref. [15] at large M_s^2/μ.

Although not associated with a phase transition, it is interesting to ask *how* the CFL phase ceases to be an insulator as it is heated. This must happen, given the phase diagram that we and the authors of Ref. [15] find, but how? At small T, the number density of charged quark quasiparticles in the CFL phase is exponentially small. Because of the interplay between $M_s \neq 0$ and the constraints of neutrality, the excitation energies of oppositely charged quasiparticles are not the same and these thermally excited quasiparticles have a net charge which must be balanced by a nonzero electron density of order μ_e^3, where μ_e is the electron chemical potential. Because

the quasiparticle densities are proportional to the quark Fermi surface area $\sim \mu^2$, where $\mu \gg \mu_e$, we show that μ_e ceases to be exponentially suppressed – rising rapidly to $\mu_e \sim M_s^2/4\mu$ – in an insulator-metal crossover that occurs in a narrow, and quite low, range of temperatures. We describe this crossover analytically in Section V. There are other charged excitations in the CFL phase, namely the pseudo-Nambu-Goldstone bosons, that are excited when the system is heated. We argue quantitatively that their effects are small.

In Section II we detail our model and approximations, stressing also those approximations used in previous work that we have not made. In Section III, we review results at $T = 0$. In Section IV, we present our results at $T \neq 0$, analyzing the phase diagram in Fig. 1 and that for other values of Δ_0. In Section V, we analyze the insulator-metal crossover that occurs when the CFL phase is heated. In Section VI, we make the connection between our work and the Ginzburg-Landau analysis quantitative. We conclude in Section VII.

II. MODEL AND APPROXIMATIONS

A. Pairing ansatz for gap parameters

We assume that the predominant diquark condensate is a Lorentz scalar (antisymmetric in Dirac indices), is antisymmetric in color (as is favored energetically), and consequently is antisymmetric in flavor. That is, we assume a condensate of the form (2). The gap parameters Δ_1, Δ_2 and Δ_3 describe a 9×9 matrix in color-flavor space that, in the basis $(ru, gd, bs, rd, gu, rs, bu, gs, bd)$, takes the form

$$\mathbf{\Delta} = \gamma_5 \cdot \begin{pmatrix} 0 & \Delta_3 & \Delta_2 & 0 & 0 & 0 & 0 & 0 & 0 \\ \Delta_3 & 0 & \Delta_1 & 0 & 0 & 0 & 0 & 0 & 0 \\ \Delta_2 & \Delta_1 & 0 & 0 & 0 & 0 & 0 & 0 & 0 \\ 0 & 0 & 0 & 0 & -\Delta_3 & 0 & 0 & 0 & 0 \\ 0 & 0 & 0 & -\Delta_3 & 0 & 0 & 0 & 0 & 0 \\ 0 & 0 & 0 & 0 & 0 & 0 & -\Delta_2 & 0 & 0 \\ 0 & 0 & 0 & 0 & 0 & -\Delta_2 & 0 & 0 & 0 \\ 0 & 0 & 0 & 0 & 0 & 0 & 0 & 0 & -\Delta_1 \\ 0 & 0 & 0 & 0 & 0 & 0 & 0 & -\Delta_1 & 0 \end{pmatrix} \tag{3}$$

We see that (gs, bd), (rs, bu) and (rd, gu) quarks pair with gap parameters Δ_1, Δ_2 and Δ_3 respectively, while the (ru, gd, bs) quarks pair among each other involving all the Δ's. The most important physics that we are leaving out by making this ansatz is pairing in which the Cooper pairs are symmetric in color, and therefore also in flavor. Diquark condensates of this form break no new symmetries, and therefore *must* arise in the CFL phase [2, 18]. However because the QCD interaction is repulsive between quarks that are symmetric in color these condensates are numerically insignificant [2, 15, 18].

B. CFL symmetries and excitations

To set the stage for our analysis, and to introduce the excitations that shall concern us, we briefly summarize the properties of the CFL phase [2]. If we set all three quark masses to zero, the diquark condensate in the CFL phase (which then has $\Delta_1 = \Delta_2 = \Delta_3$) spontaneously breaks the full symmetry group of QCD,

$$\begin{aligned} [SU(3)_{\rm color}] \times \underbrace{SU(3)_L \times SU(3)_R}_{\supset [U(1)_Q]} \times U(1)_B \\ \rightarrow \quad \underbrace{SU(3)_{C+L+R}}_{\supset [U(1)_{\tilde{Q}}]} \times \mathbb{Z}_2 \end{aligned} \tag{4}$$

where $SU(3)_{\rm color}$ and electromagnetism $U(1)_Q$ are gauged, and the unbroken $SU(3)_{c+L+R}$ subgroup consists of flavor rotations of the left and right quarks with equal and opposite color rotations, and contains an unbroken gauged "rotated electromagnetism" $U(1)_{\tilde{\rm Q}}$ [2, 19]. The CFL phase has the largest possible unbroken symmetry consistent with diquark condensation, achieved by having all nine quarks participate equally in the pairing, and this gives the maximal pairing free energy benefit. Not surprisingly, *ab initio* calculations valid at asymptotic densities confirm that the CFL phase is the ground state of QCD in the high density limit [1, 20].

The axial flavor $U(1)_A$ rotations are not a symmetry of QCD, as they are explicitly broken at all densities by instanton effects. At asymptotic densities, these effects become small but at accessible densities they cannot be neglected [2, 21, 22, 23, 24], and they shall play an important role in Section V A.

In the limit of three massless quarks described above there are 17 broken symmetry generators in the CFL phase, 8 of which become longitudinal components of massive gauge bosons and 9 of which remain as Nambu-Goldstone bosons. The massive gauge bosons have excitation energies of order $g\mu$, where the QCD gauge coupling g is not small, and we neglect them throughout. In the real world, with its two light quark flavors with masses $\lesssim 10$ MeV, and a medium-weight flavor, the strange quark, with mass $\gtrsim 100$ MeV, the eight Nambu-Goldstone bosons coming from the breaking of chiral symmetries acquire masses [1, 2, 23, 24, 25, 26], and furthermore the CFL condensate may rotate in the K^0-direction within the manifold describing these mesons [12]. We neglect the possibility of K^0-condensation throughout. We shall see in Section V A that this corresponds to assuming that the instanton contribution to the K^0 mass is comparable to Δ_0 [24, 27], which is likely the case for all but the largest Δ_0 that we consider. We must also consider the thermally excited pseudo-Nambu-Goldstone bosons, but we show in Section V A that their effects are negligible. The ninth Nambu-Goldstone boson, corresponding to the spontaneous breaking of $U(1)_B$ and hence to superfluidity, remains massless even once quark masses are taken into

account and therefore plays a crucial role in many low energy properties of the CFL phase, for example in its specific heat, thermal conductivity, neutrino opacity, and neutrino emissivity at low temperatures [27, 28, 29]. However, because it is neutral it will play no role in our analysis.

The excitations of the CFL phase that are most relevant to our considerations are the nine fermionic quasiparticles, whose excitation requires the breaking of pairs. In analyzing the response of the CFL phase to the strange quark mass at zero temperature, the quasiquark dispersion relations signal the instability corresponding to the disruption of pairing that constitutes the CFL→gCFL transition [5, 6]. These dispersion relations are even more crucial at nonzero temperature, because they determine the number densities of thermally excited quasiparticles, some of which are charged and which we shall see therefore play a crucial role in the neutrality conditions. Furthermore, these dispersion relations define the gap equations that we shall solve at nonzero temperature, again as we shall see.

C. Color and electric neutrality

Stable bulk matter must be neutral under all gauged charges, whether they are spontaneously broken or not. Otherwise, the net charge density would create large electric fields, making the energy non-extensive. In the case of the electromagnetic gauge symmetry, this simply requires zero charge density. In the case of the color gauge symmetry, the formal requirement is that a chunk of quark matter should be a color singlet, i.e., its wavefunction should be invariant under a general color gauge transformation. Color neutrality, meaning equality in the numbers of red, green and blue quarks, is a less stringent constraint. A color singlet state is also color neutral, whereas the opposite is not necessarily true. However it has been shown that the projection of a color neutral state onto a color singlet state costs no extra free energy in the thermodynamic limit [30]. Analyzing the consequences of the requirement of color neutrality therefore suffices for our purposes.

In nature, electric and color neutrality are enforced by the dynamics of the electromagnetic and QCD gauge fields, whose zeroth components serve as chemical potentials which take on values that enforce neutrality [4, 31]. Since we are limiting ourselves to color neutrality and not color singletness we have to consider only the $U(1)\times U(1)$ diagonal subgroup of the color gauge group. This subgroup is generated by the diagonal generators $T_3 = \mathrm{diag}(\frac{1}{2}, -\frac{1}{2}, 0)$ and $T_8 = \mathrm{diag}(\frac{1}{3}, \frac{1}{3}, -\frac{2}{3})$ of the $SU(3)$ gauge group. Electromagnetism is generated by $Q = \mathrm{diag}(\frac{2}{3}, -\frac{1}{3}, -\frac{1}{3})$ in flavor space (u, d, s). The zeroth components of the respective gauge fields serve as chemical potentials μ_3 and μ_8 coupled to T_3 and T_8 charges, and as an electrostatic potential μ_e coupled to the *negative* electric charge Q. (We make this last choice so that $\mu_e > 0$ corresponds to a density of electrons, not positrons.) The dynamics of the gauge potentials then require that the charge densities, which are the derivatives of the free energy with respect to the chemical potentials, must vanish:

$$\begin{aligned} n_Q &= \frac{\partial\Omega}{\partial\mu_e} = 0 \\ n_3 &= -\frac{\partial\Omega}{\partial\mu_3} = 0 \\ n_8 &= -\frac{\partial\Omega}{\partial\mu_8} = 0\ . \end{aligned} \tag{5}$$

In an NJL model with fermions but no gauge fields that we shall employ, one has to introduce the chemical potentials μ_e, μ_3 and μ_8 "by hand" in order to enforce color and electric neutrality in the same way that gauge field dynamics does in QCD [4].

A generic diquark condensate will be neither electrically nor color neutral, so it will spontaneously break these gauge symmetries. However it may be neutral under a linear combination of electromagnetism and color. Indeed, any condensate of the form (2) is neutral with respect to the "rotated electromagnetism" generated by $\tilde{Q} = Q - T_3 - \frac{1}{2}T_8$, so $U(1)_{\tilde{Q}}$ is never broken. This means that the corresponding gauge boson (the "$\tilde{Q}$-photon"), a mixture of the ordinary photon and one of the gluons, remains massless. In both the CFL and gCFL phases, the rest of the $SU(3)_{\rm color} \times U(1)_Q$ gauge group is spontaneously broken, meaning that the combination of the photon and gluons orthogonal to the $\tilde{Q}$-photon, and all the other gluons, become massive by the Higgs mechanism.

In the CFL phase at $T = 0$, many consequences of the neutrality equations can be analyzed in a model-independent way [4]. A central result is that the free energy Ω is independent of

$$\mu_{\tilde{Q}} = -\tfrac{4}{9}\big(\mu_e + \mu_3 + \tfrac{1}{2}\mu_8\big)\ , \tag{6}$$

the chemical potential for $\tilde{Q}$-charge, as long as $\mu_{\tilde{Q}}$ is not so large that it disrupts CFL pairing. This means that the CFL phase is a $\tilde{Q}$-insulator at $T = 0$ [32]. Translating back into μ_e, μ_3 and μ_8, this means that two of these three can be fixed as functions of the third:

$$\mu_3 = \mu_e, \tag{7}$$

$$\mu_8 = -\frac{M_s^2}{2\mu} + \frac{\mu_e}{2}, \tag{8}$$

where μ_e can lie anywhere within the range $-\Delta_2 + \frac{M_s^2}{2\mu} < \mu_e < +\Delta_3$. If the lower (upper) bound of this range is violated *rs-bu* (*rd-gu*) pairing is disrupted: this range can be thought of as the bandgap for the CFL insulator [5]. The free energy Ω has a plateau within this range of $\mu_{\tilde{Q}}$. Electrons add a new term $\sim \mu_e^4$ to Ω, adding a gentle curvature to the plateau, and selecting $\mu_e = 0$, meaning zero electron density, as the correct solution for neutral

CFL matter at $T = 0$. (μ_3 and μ_8 are then given by (7,8) with $\mu_e = 0$.) At finite temperature where quasiquarks with non-trivial $\tilde{Q}$ are excited, we shall see that because Ω has an only-very-gently-curved plateau, it will not take much thermal excitation of quasiquarks to shift μ_e significantly away from zero.

D. A Model for the Thermodynamic Potential

We are interested in physics at non-asymptotic densities, and therefore cannot use weak-coupling methods. We are interested in physics at zero temperature and high density, at which the fermion sign problem is acute and the current methods of lattice QCD can therefore not be employed. For this reason, we need to introduce a model in which the interaction between quarks is simplified, while still respecting the symmetries of QCD, and in which the effects of M_s, μ_e, μ_3, μ_8 and T on CFL pairing can all be investigated. The natural choice is to model the interactions between quarks using a point-like four-fermion interaction, which we shall take to have the quantum numbers of single-gluon exchange. We work in Euclidean space. Our partition function $\mathcal{Z}$ and free energy density Ω are then defined by

$$\begin{aligned} \mathcal{Z} &= \mathrm{e}^{-\beta V\Omega} = \mathcal{N}\int \mathcal{D}\bar{\psi}\mathcal{D}\psi \exp\Bigl(\int \mathcal{L}(x)\, d^4x\Bigr) \\ \mathcal{L}(x) &= \bar{\psi}(i\partial\!\!\!/ + \mu\!\!\!/ - \boldsymbol{M})\psi - \frac{3}{8}G(\bar{\psi}\Gamma^A_\mu\psi)(\bar{\psi}\Gamma^\mu_A\psi) \end{aligned} \tag{9}$$

where the fields live in a box of volume V and Euclidean time length $\beta = 1/T$, and $\mu\!\!\!/ = \boldsymbol{\mu}\gamma_4$. The interaction vertex has the color, flavor, and spin structure of the QCD gluon-quark coupling, $\Gamma^A_\mu = \gamma_\mu T^A$ with the T_A normalized such that $\mathrm{Tr}\, T_A T_B = 2\delta_{AB}$. The mass matrix $\boldsymbol{M} = \mathrm{diag}(0, 0, M_s)$ in flavor space. The chemical potential $\boldsymbol{\mu}$ is a diagonal color-flavor matrix depending on μ, μ_e, μ_3 and μ_8. The normalization of the four-fermion coupling $3G/8$ is as in the first paper in Ref. [1]. In real QCD, the ultraviolet modes decouple because of asymptotic freedom but, in the NJL model, we have to add this feature by hand, through a UV momentum cutoff Λ in the momentum integrals. The model therefore has two parameters, the four-fermion coupling G and the three-momentum cutoff Λ, but it is more useful to parameterize the interaction in terms of a physical quantity, namely the CFL gap parameter at $M_s = T = 0$ at a reference chemical potential that we shall take to be 500 MeV. We shall call this reference gap Δ_0. We have checked that if we vary the cutoff Λ by 20% while simultaneously varying the bare coupling G so as to keep Δ_0 fixed, then our results change by a few percent at most. All the results that we present are for $\Lambda = 800$ MeV. Most of the results that we present are for a coupling strength chosen such that $\Delta_0 = 25$ MeV, but we shall also discuss results obtained with stronger couplings for which $\Delta_0 = 40$ MeV and $\Delta_0 = 100$ MeV.

The free energy Ω obtained from the Lagrangian (9) upon making the ansatz (2) for the diquark condensate and working in the mean field approximation has been presented in Ref. [6]. More sophisticated derivations exist in the literature [1], but since we are assuming that the only condensate is of the form (2) we can Fierz transform the interaction to yield products of terms that appear in (2), and discard all the other terms that arise in the Fierz transformed interaction which would anyway vanish after making the mean field approximation. This yields

$$\mathcal{L}_{\mathrm{int}} = \frac{G}{4}\sum_\eta (\bar{\psi}P_\eta\bar{\psi}^T)(\psi^T\bar{P}_\eta\psi)\ , \tag{10}$$

where

$$(P_\eta)^{\alpha\beta}_{ij} = C\gamma_5\epsilon^{\alpha\beta\eta}\epsilon_{ij\eta} \quad (\text{no sum over } \eta) \tag{11}$$

and $\bar{P}_\eta = \gamma_4 P_\eta^\dagger \gamma_4$. The index η labels the pairing channel: $\eta = 1, 2$, and 3 correspond to d-s pairing, u-s pairing, and u-d pairing. The gap parameters can then be defined precisely as

$$\Delta_\eta = \tfrac{1}{2}G\langle\psi^{\mathrm{T}}\bar{P}_\eta\psi\rangle\ . \tag{12}$$

As derived in Ref. [6], the free energy can then be written as

$$\begin{aligned} \Omega = &-\frac{1}{4\pi^2}\int_0^\Lambda dp\, p^2 \sum_j \Bigl\{|\varepsilon_j(p)| + 2T\ln\bigl(1+\mathrm{e}^{-|\varepsilon_j(p)|/T}\bigr)\Bigr\} \\ &+ \frac{1}{G}\bigl(\Delta_1^2+\Delta_2^2+\Delta_3^2\bigr) - \frac{\mu_e^4}{12\pi^2} - \frac{\mu_e^2T^2}{6} - \frac{7\pi^2T^4}{180}\ , \end{aligned} \tag{13}$$

where the electron contribution for $T \neq 0$ has been included. The functions $\varepsilon_j(p)$ are the dispersion relations for the fermionic quasiparticles. They are not explicitly T-dependent, but they do depend on the Δ's and μ's which are T-dependent. The quasiquark dispersion relations $\varepsilon_j(p)$ are the values of the energy at which the propagator diverges,

$$\det S^{-1}(-i\varepsilon_j(p), p) = 0\ . \tag{14}$$

Here, the inverse propagator S^{-1} is the 72×72 matrix

$$S^{-1}(p) = \begin{pmatrix} p\!\!\!/ + \mu\!\!\!/ - \boldsymbol{M} & P_\eta\Delta_\eta \\ \bar{P}_\eta\Delta_\eta & (p\!\!\!/ - \mu\!\!\!/ + \boldsymbol{M})^T \end{pmatrix} \tag{15}$$

that acts on Nambu-Gor'kov spinors

$$\Psi = \begin{pmatrix} \psi(p) \\ \bar{\psi}^T(-p) \end{pmatrix}, \quad \bar{\Psi} = \begin{pmatrix} \bar{\psi}(p) & \psi^T(-p) \end{pmatrix}. \tag{16}$$

The sum in (13) is understood to run over 36 roots, because the Nambu-Gor'kov formalism has artificially made each $|\varepsilon_j|$ doubly degenerate. There is a further (physical) degeneracy coming from spin, meaning that there are only 18 distinct dispersion relations to be found. The free energy of any solution to the gap equations obtained

from this mean field free energy is the same as that obtained from the Cornwall-Jackiw-Tomboulis effective potential [33], with the mean field approximation implemented via dropping the contribution of 2PI diagrams.

We shall evaluate Ω numerically, meaning that at every value of the momentum p we must find the zeros of the inverse propagator. In order to do this numerically, we follow Ref. [11] and note that it is equivalent and faster to find the eigenvalues of the "Dirac Hamiltonian density" $\mathcal{H}(p)$, which is related to S^{-1} by

$$\det S^{-1}(p_4,p) = \det\Big[\gamma^4\big(ip_4 - \mathcal{H}(p)\big)\Big] \ , \qquad (17)$$

which makes it clear that eigenvalues of $\mathcal{H}(p)$ are zeros of S^{-1}. Like S^{-1}, the Dirac Hamiltonian $\mathcal{H}(p)$ is a 72×72 matrix in color, flavor, spin, and Nambu-Gor'kov space. This matrix can be decomposed into 4 blocks – three 16×16 matrices for the (*rd-gu*), (*rs-bu*) and (*gs-bd*) pairing sectors, and one 24×24 matrix for the (*ru-gd-bs*) sector. The absolute values of the eigenvalues are quadruply degenerate due to the Nambu-Gor'kov doubling and the spin degeneracy.

We have found considerably simpler expressions for the (*rd-gu*), (*rs-bu*) and (*gs-bd*) sectors. The calculation becomes easier if one adopts a different choice of Nambu-Gor'kov basis, i.e. $\Psi = (\psi(p), C\bar{\psi}^{\rm T}(-p))^{\rm T}$ as in Ref. [34]. Then the Nambu-Gor'kov and spin degeneracies are manifest, as the 16×16 matrix separates into 4×4 blocks with the form

$$\mathcal{H}_{(gs\text{-}bd)} = \begin{pmatrix} -\mu_{bd} & p & 0 & i\Delta_1 \\ p & -\mu_{bd} & -i\Delta_1 & 0 \\ 0 & i\Delta_1 & \mu_{gs}+M_s & p \\ -i\Delta_1 & 0 & p & \mu_{gs}-M_s \end{pmatrix} \qquad (18)$$

for the (*gs-bd*) sector and likewise for other sectors. Each of the 4 eigenvalues of this matrix, and of its counterparts for the other sectors, contributes twice (for spin) in the sum in (13). The quark chemical potentials occurring in (18) and below are defined straightforwardly:

$$\begin{aligned}
\mu_{ru} &= \mu - \tfrac{2}{3}\mu_e + \tfrac{1}{2}\mu_3 + \tfrac{1}{3}\mu_8, \\
\mu_{gd} &= \mu + \tfrac{1}{3}\mu_e - \tfrac{1}{2}\mu_3 + \tfrac{1}{3}\mu_8, \\
\mu_{bs} &= \mu + \tfrac{1}{3}\mu_e - \tfrac{2}{3}\mu_8, \\
\mu_{rd} &= \mu + \tfrac{1}{3}\mu_e + \tfrac{1}{2}\mu_3 + \tfrac{1}{3}\mu_8, \\
\mu_{gu} &= \mu - \tfrac{2}{3}\mu_e - \tfrac{1}{2}\mu_3 + \tfrac{1}{3}\mu_8, \\
\mu_{rs} &= \mu + \tfrac{1}{3}\mu_e + \tfrac{1}{2}\mu_3 + \tfrac{1}{3}\mu_8, \\
\mu_{bu} &= \mu - \tfrac{2}{3}\mu_e - \tfrac{2}{3}\mu_8, \\
\mu_{gs} &= \mu + \tfrac{1}{3}\mu_e - \tfrac{1}{2}\mu_3 + \tfrac{1}{3}\mu_8, \\
\mu_{bd} &= \mu + \tfrac{1}{3}\mu_e - \tfrac{2}{3}\mu_8 \ .
\end{aligned} \qquad (19)$$

In the (*ru-gd-bs*) sector, we could not find any simple way to make the spin degeneracy manifest, but the Nambu-Gor'kov degeneracy is manifest as the 24×24 matrix separates into 12×12 blocks with the form

$$\mathcal{H}_{(ru\text{-}gd\text{-}bs)} = \begin{pmatrix}
-\mu_{ru} & p & 0 & -i\Delta_3 & 0 & -i\Delta_2 & 0 & 0 & 0 & 0 & 0 & 0 \\
p & -\mu_{ru} & i\Delta_3 & 0 & i\Delta_2 & 0 & 0 & 0 & 0 & 0 & 0 & 0 \\
0 & -i\Delta_3 & \mu_{gd} & p & 0 & 0 & 0 & -i\Delta_1 & 0 & 0 & 0 & 0 \\
i\Delta_3 & 0 & p & \mu_{gd} & 0 & 0 & i\Delta_1 & 0 & 0 & 0 & 0 & 0 \\
0 & -i\Delta_2 & 0 & 0 & \mu_{bs}+M_s & p & 0 & 0 & 0 & -i\Delta_1 & 0 & 0 \\
i\Delta_2 & 0 & 0 & 0 & p & \mu_{bs}-M_s & 0 & 0 & i\Delta_1 & 0 & 0 & 0 \\
0 & 0 & 0 & -i\Delta_1 & 0 & 0 & -\mu_{bs}+M_s & p & 0 & 0 & 0 & -i\Delta_2 \\
0 & 0 & i\Delta_1 & 0 & 0 & 0 & p & -\mu_{bs}-M_s & 0 & 0 & i\Delta_2 & 0 \\
0 & 0 & 0 & 0 & 0 & -i\Delta_1 & 0 & 0 & -\mu_{gd} & p & 0 & -i\Delta_3 \\
0 & 0 & 0 & 0 & i\Delta_1 & 0 & 0 & 0 & p & -\mu_{gd} & i\Delta_3 & 0 \\
0 & 0 & 0 & 0 & 0 & 0 & 0 & -i\Delta_2 & 0 & -i\Delta_3 & \mu_{ru} & p \\
0 & 0 & 0 & 0 & 0 & 0 & i\Delta_2 & 0 & i\Delta_3 & 0 & p & \mu_{ru}
\end{pmatrix} . \qquad (20)$$

The 12 eigenvalues of this matrix each contribute once in the sum in (13). They occur in degenerate pairs due to spin.

A stable, neutral phase must minimize the free energy (13) with respect to variation of the three gap parameters Δ_1, Δ_2, Δ_3, meaning it must satisfy

$$\frac{\partial\Omega}{\partial\Delta_1} = 0, \qquad \frac{\partial\Omega}{\partial\Delta_2} = 0, \qquad \frac{\partial\Omega}{\partial\Delta_3} = 0 \ , \qquad (21)$$

and it must satisfy the three neutrality conditions (5). The gap equations (21) and neutrality equations (5) form a system of six coupled integral equations with unknowns

the three gap parameters and μ_e, μ_3 and μ_8. We have solved these equations numerically at a grid of values of T and M_s^2/μ. We evaluate Ω using (13), finding the ε_j by determining the eigenvalues of the matrices specified explicitly above. We evaluate partial derivatives of Ω using finite difference methods. (We used three and five point finite difference evaluations of derivatives, with the interval in the Δ or μ with respect to which Ω is being differentiated taken as 0.04 MeV.) We have worked entirely with $\mu = 500$ MeV, varying M_s^2/μ by varying M_s, and have worked at three values of the coupling G chosen so that Δ_0, the gap parameter at $M_s = T = 0$, takes on the values $\Delta_0 = 25$, 40 and 100 MeV.

E. Approximations made and not made

Having described our calculation in explicit detail, we close this section by enumerating the approximations that we are making, and stressing several that we have not made.

We have made the following approximations:

1. We work throughout in a mean field approximation. Gauge field fluctuations will surely be important, and must be included in future work.

2. We neglect contributions to the condensates that are symmetric in color and flavor: these are known to be present and small, smaller than the contributions that we include by at least an order of magnitude [2, 15, 18].

3. We choose light quark masses $M_u = M_d = 0$ and we treat the constituent strange quark mass M_s as a parameter, rather than solving for an $\langle \bar{s}s \rangle$ condensate. These approximations should be improved upon, along the lines of Refs. [11, 34]. In future studies in which the $\langle \bar{q}q \rangle$ condensates are solved for dynamically, the six-quark 't Hooft interaction induced by instantons must be included, since it introduces terms of the form $\langle \bar{s}s \rangle |\Delta_3|^2$, for example.

4. We ignore meson condensation in both the CFL phase and gCFL phases. We shall see in Section V A that in the CFL phase this means that we are assuming that the instanton contribution to the K^0 mass is comparable to or larger than Δ_0 [24, 27]. Meson condensation in the gCFL phase has yet to be analyzed.

We expect that these approximations have quantitative effects, but none preclude a qualitative understanding of the phase diagram.

The authors of Refs. [5, 6] made further simplifying assumptions. They worked only to leading nontrivial order in Δ_1, Δ_2, Δ_3, μ_e, μ_3 and μ_8. They neglected the effects of antiparticles. And, most serious, they incorporated M_s only via its leading effect, namely as an effective shift $-M_s^2/\mu$ in the chemical potentials of the strange quarks. This limits the regime of applicability of their results to $M_s \ll \mu$. For $\Delta_0 \sim 100$ MeV, there is pairing even at $M_s \gtrsim \mu$ and our calculation runs into no difficulties in this regime. (We shall show some results, even though this likely corresponds to such small μ that in reality the hadronic phase has taken over.) In the next section, we shall present our $T = 0$ results. Those with $\Delta_0 = 25$ MeV, as in Refs. [5, 6], are in very good agreement with the results of Refs. [5, 6]. This provides quantitative evidence for the validity of the approximations made in Refs. [5, 6] at $\Delta_0 = 25$ MeV.

III. ZERO TEMPERATURE RESULTS

In this section we shall present the results of our model analysis at $T = 0$. Here and throughout this paper, we set $\mu = 500$ MeV corresponding to a baryon density about ten times that in nuclear matter, which is within the range of expectations for the density at the center of compact stars. In reality, both M_s and Δ_0 vary with μ, and our knowledge of both is uncertain. Our model is by construction well-suited to study the disruptive effects of M_s on pairing but it is not adequate to fix the density-dependent values of either M_s or Δ_0 quantitatively. In this study, therefore, as in Refs. [4, 5, 6, 15] we treat both M_s and Δ_0 simply as parameters. We shall plot our results versus M_s^2/μ, rather than versus M_s itself, because the strength of the disruptive effects introduced by the strange quark mass are characterized by M_s^2/μ. For example, the splitting between Fermi surfaces in unpaired quark matter is of order $M_s^2/4\mu$, and the CFL→gCFL transition occurs where $M_s^2/\mu \simeq 2\Delta_1$. Although we only present results at a single value of μ, because the effects of M_s are controlled by M_s^2/μ, and because in reality M_s is itself a decreasing function of μ, one can think of our plots as giving a qualitative description of the effects of varying μ, with high density at small M_s^2/μ and low density at large M_s^2/μ. This description is only qualitative because our plots are each made with some fixed value of Δ_0, whereas in reality Δ_0 depends on μ.

We begin by choosing the four fermion coupling G so that $\Delta_0 = 25$ MeV, as in Refs. [5, 6]. The solid curves in Fig. 2 show the gap parameters as a function of M_s^2/μ, and those in Fig. 3 show the chemical potentials. These plots are in very good agreement with those of Refs. [5, 6], indicating that the approximations made in that paper that we have dispensed with here, chiefly the small-M_s^2/μ^2 assumption, were good approximations for $\Delta_0 = 25$ MeV. For small M_s^2/μ, we see the CFL phase with $\Delta_1 = \Delta_2 \simeq \Delta_3$. The small difference between $\Delta_1 = \Delta_2$ and Δ_3, less than 2% everywhere within the CFL phase, is an example of an effect that we can see but that cannot be seen in the small-M_s^2/μ^2 approximation in which M_s is approximated as a shift in the chemical potential for the strange quarks [5, 6]. The CFL→gCFL transition occurs at $M_s^2/\mu = 46.8$ MeV, which is very close to $2\Delta_1$, since $\Delta_1 = 23.2$ MeV at

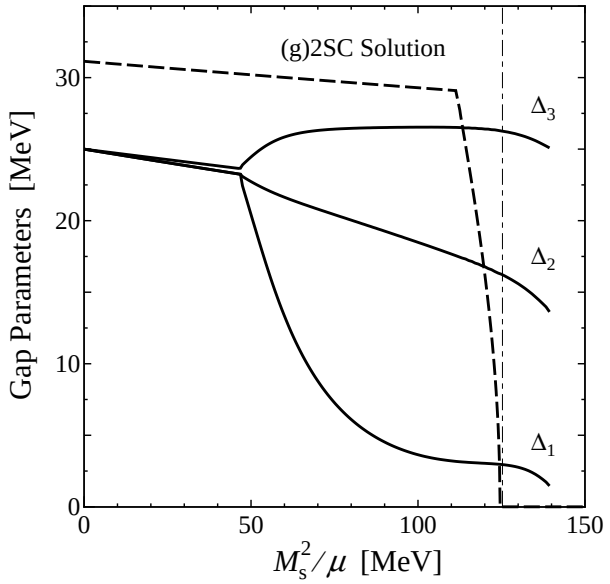

FIG. 2: Gap parameters Δ_1, Δ_2 and Δ_3 as a function of M_s^2/μ at $T = 0$. The solid curves show the CFL/gCFL solution, with the CFL→gCFL transition occurring where $M_s^2/\mu \simeq 2\Delta_1$. There is a first order phase transition between the gCFL phase and unpaired quark matter at $M_s^2/\mu = 125.3$ MeV, denoted by the the thin vertical line. To the right of this line, the gCFL solution is metastable. We also find a neutral 2SC solution, with Δ_3 given by the dashed curve in the figure, which undergoes a transition to the gapless 2SC phase of Refs. [35] at $M_s^2/\mu = 112$ MeV. However, from Fig. 4 we see that the (g)2SC solution is everywhere metastable, having a larger free energy than the (g)CFL solution at the same M_s^2/μ.

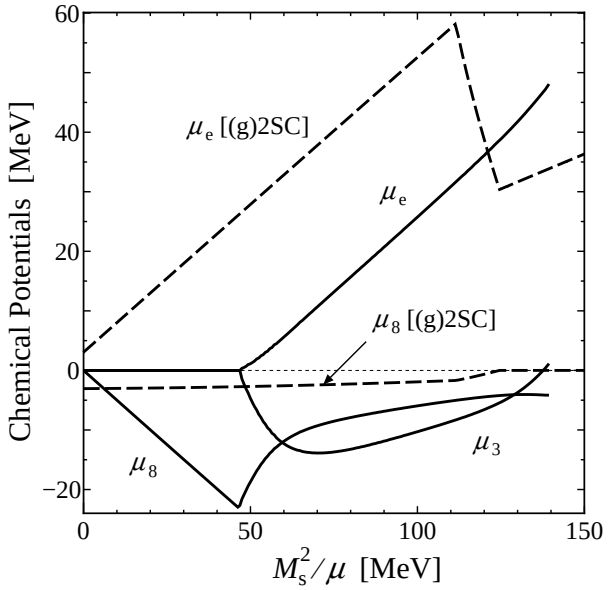

FIG. 3: Chemical potentials μ_e, μ_3 and μ_8 as a function of M_s^2/μ at $T = 0$, for the (g)CFL and (g)2SC solutions of Fig. 2. ($\mu_3 = 0$ in the (g)2SC solution and so is not shown.) Beyond the M_s^2/μ at which the g2SC solution ends, the dashed curve shows the chemical potentials ($\mu_e \neq 0$ and $\mu_8 = 0$) for neutral unpaired quark matter.

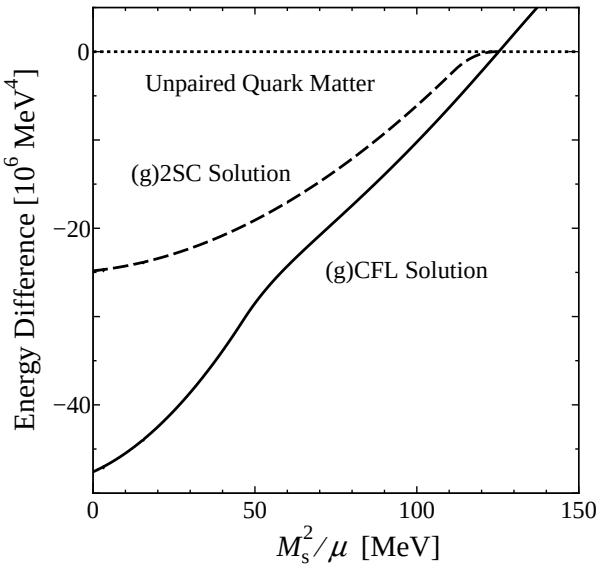

FIG. 4: Free energies of the (g)CFL and (g)2SC solutions of Fig. 2 at $T = 0$, relative to that of neutral unpaired quark matter.

$M_s^2/\mu = 46.8$ MeV. We see from Fig. 3 that $\mu_e \neq 0$ in the gCFL phase, indicating a nonzero electron density. As discussed in detail in Refs. [5, 6], the negative $\tilde{Q}$-charge of the electrons is balanced by that of unpaired bu quarks, which have $\tilde{Q} = +1$, occurring in a narrow shell in momentum space. There is a larger shell in momentum space, whose width grows with increasing M_s^2/μ in the gCFL phase, within which there are unpaired bd-quarks. This "blocking region" of momentum space does not contribute in the Δ_1 gap equation, and Δ_1 is consequently driven down. The gap equations and neutrality conditions are all coupled, and the consequences of the reduction in Δ_1 and the increase in μ_e are manifest in all the curves in Figs. 2 and 3.

As M_s^2/μ increases further, the gCFL solution eventually ceases to exist at $M_s^2/\mu = 139$ MeV. The gCFL solution to the gap equations is a minimum of Ω with respect to variation of the Δ's for $M_s^2/\mu < 139$ MeV, becomes an inflection point at $M_s^2/\mu = 139$ MeV, and for larger M_s^2/μ there is no such solution. This is analyzed in greater detail in Refs. [5, 6]. The fact that the gCFL solution disappears indicates that there should be some other minimum with lower free energy, and indeed as shown in Fig. 4 we find that a first-order phase transition at which the gCFL free energy crosses above that of unpaired quark matter has occurred at $M_s^2/\mu = 125$ MeV, indicated in Fig. 2 by the vertical line. In Ref. [6], the first order phase transition and the termination of the gCFL phase at a point of inflection of the free energy occur at $M_s^2/\mu = 130$ MeV and $M_s^2/\mu = 144$ MeV respectively. Therefore, the errors in these quantities introduced by the small-M_s^2/μ^2 approximation, used in Refs. [5, 6] but

not here, are about 4% at these values of M_s^2/μ.

As in Ref. [6], we find an additional neutral 2SC solution, whose gap parameter Δ_3 and free energy are shown in Figs. 2 and 4. At $M_s = 0$, the 2SC gap is $2^{1/3}\Delta_0$ [1, 22]. For M_s^2/μ below the 2SC→g2SC transition at $M_s^2/\mu = 112$ MeV, *rd-gu* and *ru-gd* pairing occur at all momenta; above this transition, in the gapless 2SC phase [35, 36], there is a blocking region [37] in momentum space in which one finds unpaired *rd* and *gd* quarks, and Δ_3 drops precipitously. An analogue of the g2SC phase [38] (and in fact an analogue of the gCFL phase [39]) were first analyzed in contexts in which they were metastable, but it was shown in Ref. [35] that the g2SC phase could be stabilized in two-flavor quark matter by the constraints of neutrality. However, we see in Fig. 4 that in this three-flavor quark matter setting, the (g)2SC solution everywhere has a larger free energy than the (g)CFL solution at the same M_s^2/μ, and is therefore metastable. The value of M_s^2/μ at which $\Delta_3 \to 0$ in the g2SC solution is less than 1 MeV below the M_s^2/μ at which the gCFL phase becomes metastable. In contrast, in Ref. [6] the g2SC solution persists to an M_s^2/μ that is less than 1 MeV above that at which the gCFL phase free energy crosses that of unpaired quark matter. This is the one instance where the small-M_s^2/μ^2 approximation made in Ref. [6] leads one (slightly) astray, as it predicts a (very narrow) M_s^2/μ-window in which the g2SC phase is favored and we find no such window. However, we shall see below that the physics at values of M_s^2/μ that are this large compared to Δ_0 is anyway not robust, changing qualitatively with increasing Δ_0.

We now investigate how our zero temperature results change if we vary the strength of the coupling, and hence Δ_0. In Fig. 5, we show the gap parameters as a function of M_s^2/μ with $\Delta_0 = 40$ MeV. We have changed the scale on both the horizontal and vertical axes by the same factor of 40/25. We see that the CFL→gCFL transition again occurs at $M_s^2/\mu \simeq 2\Delta_1$, and that the shape of the curves in the gCFL region is qualitatively as before, when suitably rescaled. However, at large values of M_s^2/μ we now find a g2SC window: the gCFL free energy crosses above that of the g2SC phase — whose gap parameter Δ_3 is also shown in Fig. 5 — at the vertical line in the figure, and the g2SC gap vanishes only at a larger M_s^2/μ. (We have located the vertical line by comparing free energies, as we did in Fig. 4, but we shall not give the figure.)

If we reduce Δ_0 from 25 MeV, rather than increasing it, and rescale both axes of Fig. 2 by the same factor by which we reduce Δ_0, we obtain a figure that looks qualitatively like Fig. 2. We conclude that stronger interaction tends to favor a g2SC window at large values of M_s^2/μ, whereas weaker interaction disfavors it. The boundary between the two cases is at $\Delta_0 = 25$ MeV in our model.

It is interesting to ask what happens at still larger Δ_0. We show the gap parameters in our model with $\Delta_0 = 100$ MeV in Fig. 6. We see the CFL→gCFL transition at $M_s^2/\mu = 2\Delta_1$ once again. The physics at and

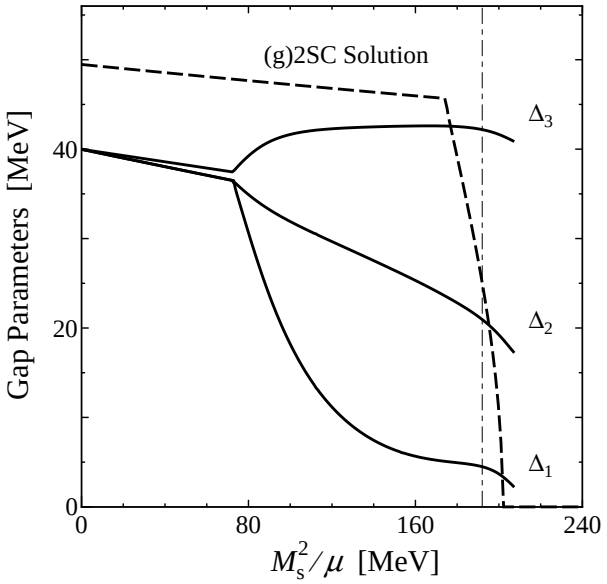

FIG. 5: Gap parameters for a stronger interaction than that in Fig. 2, chosen such that $\Delta_0 = 40$ MeV for $M_s = 0$. As in Fig. 2, the CFL→gCFL transition occurs where $M_s^2/\mu \simeq 2\Delta_1$. Here, however, the gCFL phase becomes metastable (at the thin vertical line) at a value of M_s^2/μ above which there is a g2SC solution. There is a first order gCFL→g2SC transition at the thin vertical line, followed at a larger M_s^2/μ by a second order transition at which the g2SC gap Δ_3 vanishes.

beyond the large-M_s^2/μ boundary of the gCFL regime is now qualitatively different. This regime corresponds either to very large values of M_s, or else to such small values of μ that the hadronic phase will likely have taken over, making the right half of this plot somewhat academic. One reason it is of interest, however, is simply the fact that we can draw it: had we made a small M_s^2/μ^2 approximation as in Refs. [5, 6, 15], this regime would be inaccessible. The figure shows a sequence of phases as M_s^2/μ is increased above the gCFL phase: (i) the gCFL phase ends at a second order phase transition at which $\Delta_1 \to 0$, above which we find a uSC window in which both Δ_2 and Δ_3 remain nonzero; (ii) next, $\Delta_2 \to 0$ at a second order phase transition at which the uSC phase is succeeded by the 2SC phase; (iii) finally, there is a 2SC→g2SC transition. This sequence of phases agrees with that found in Ref. [15] at large Δ_0, in a calculation done using a small-M_s^2/μ^2 approximation pushed beyond its regime of validity. Our present calculation can be extended (within its model context) to arbitrarily large M_s. Indeed, as can be seen in Fig. 7 we find a transition to two-flavor quark matter, with zero strange quark density, at $M_s = 547$ MeV, corresponding to $M_s^2/\mu = 598$ MeV. Below this M_s, we find the g2SC phase with unpaired strange quarks. Above this value of M_s, we have two-flavor g2SC quark matter and further increase in M_s has no effect on the physics.

As Δ_0 is increased from 40 MeV to 100 MeV, going

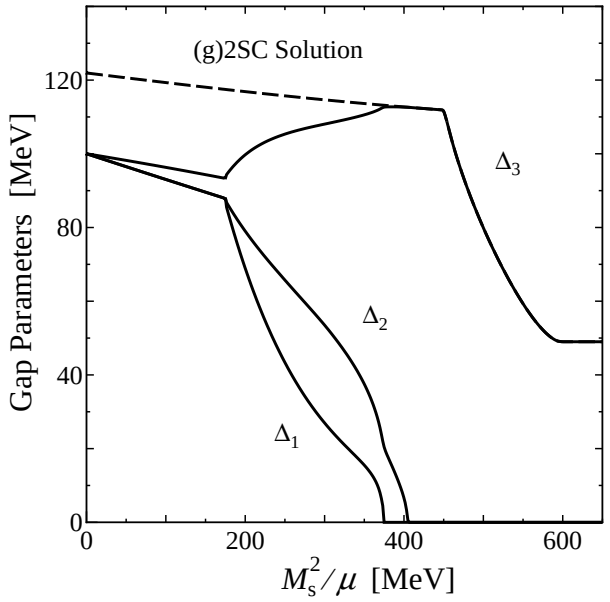

FIG. 6: Gap parameters for a still stronger interaction, with $\Delta_0 = 100$ MeV for $M_s = 0$. As in Fig. 2, the CFL→gCFL transition occurs where $M_s^2/\mu \simeq 2\Delta_1$. At $M_s^2/\mu = 375$ MeV, Δ_1 vanishes at a second order gCFL→uSC transition. Then, at $M_s^2/\mu = 405$ MeV, Δ_2 vanishes at a second order uSC→2SC transition. At $M_s^2/\mu = 449$ MeV, there is a second order 2SC→g2SC transition. And finally, for $M_s^2/\mu > 598$ MeV, corresponding to $M_s > 547$ MeV, there are no more strange quarks present in the system, as shown explicitly in Fig. 7, and further increase in M_s changes nothing.

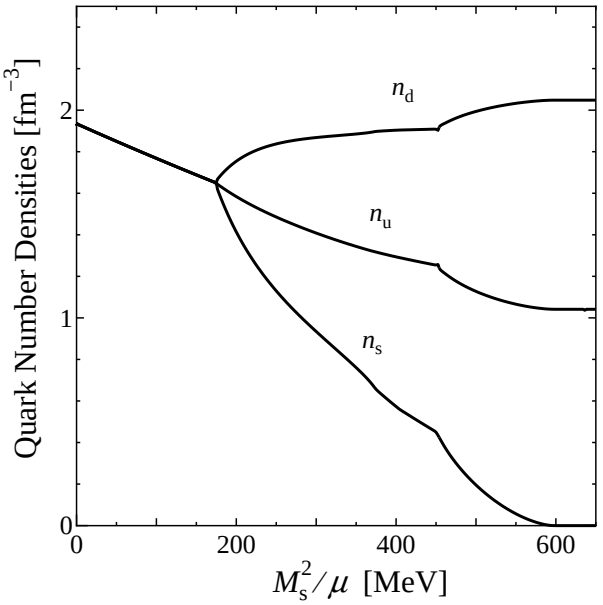

FIG. 7: Number densities of quarks with flavors u, d and s (in each case summed over the three colors) as a function of M_s^2/μ. All parameters are as in Fig. 6, with $\Delta_0 = 100$ MeV. We see that the number densities are equal only in the CFL phase, and see that for $M_s^2/\mu > 598$ MeV there are no strange quarks present.

from Fig. 5 to Fig. 6, the first qualitative change to occur is that the gCFL phase ends at a second order transition at which $\Delta_1 \to 0$, instead of ending at a first order transition. Above this Δ_0, the phase diagram includes a uSC window separated from the (g)2SC phase by a first order phase transition. At a somewhat larger Δ_0, this first order phase transition becomes second order. At a still larger Δ_0, the interaction is strong enough to have g2SC pairing in the two flavor quark matter that our model describes for $M_s \to \infty$, and the physics is as in Fig. 6.

IV. THE PHASE DIAGRAM AT NONZERO TEMPERATURE

We now explore the solutions to the gap equations and neutrality conditions at nonzero temperatures. As in the previous section, we begin with a coupling chosen so that $\Delta_0 = 25$ MeV. The phase diagram for this value of the coupling is given in Fig. 1, to which the reader should refer in this section. We constructed Fig. 1 by first making plots of the gap parameters and chemical potentials versus M_s^2/μ at many values of T, and versus T at many values of M_s^2/μ. In this Section, we present and discuss several of these "sections" of Fig. 1, enough to understand the many features of the phase diagram. We then show phase diagrams for $\Delta_0 = 40$ and 100 MeV.

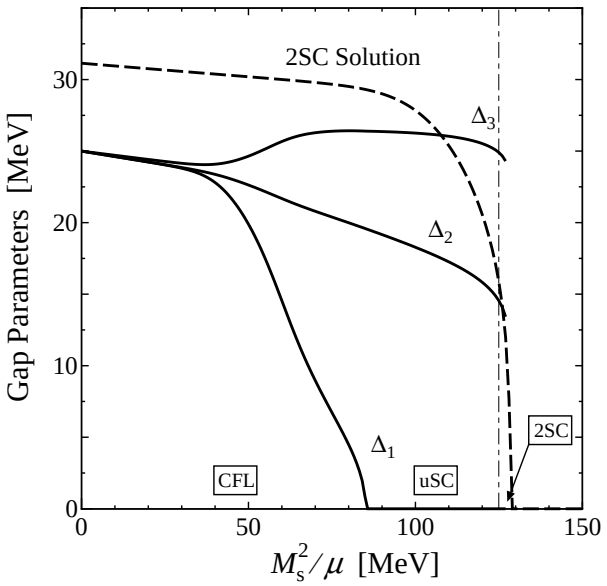

FIG. 8: Gap parameters as a function of M_s^2/μ at $T = 2$ MeV, with all other parameters as in Fig. 2.

We start by turning on a small temperature, $T = 2$ MeV, and seeing how the plots of gaps and chemical potentials, shown in Figs. 8 and 9, change from those at zero temperature, Figs. 2 and 3. We see many inter-

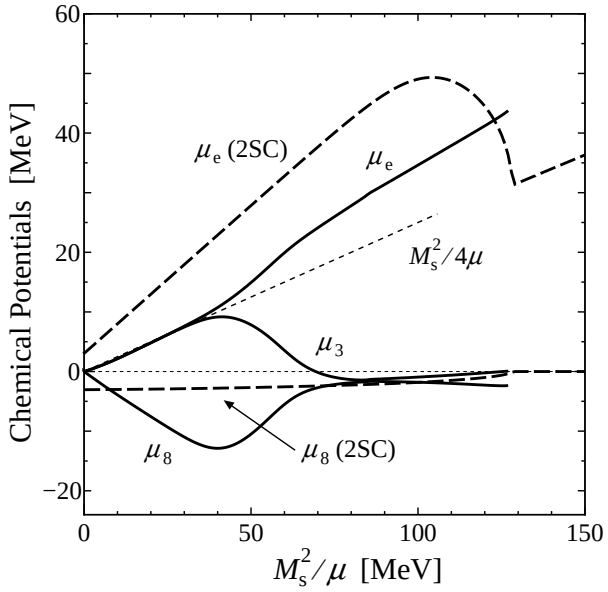

FIG. 9: Chemical potentials as a function of M_s^2/μ at $T = 2$ MeV, with all other parameters as in Fig. 3. At small M_s^2/μ, μ_e and μ_3 are close to $M_s^2/4\mu$.

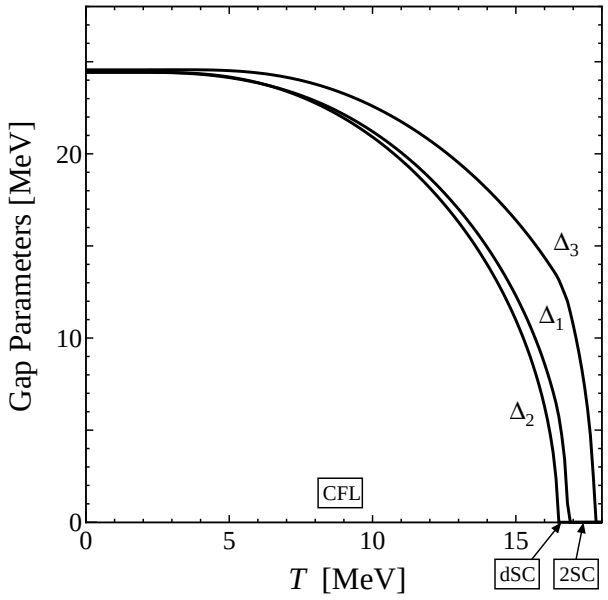

FIG. 10: Gap parameters as a function of T at $M_s^2/\mu = 15$ MeV.

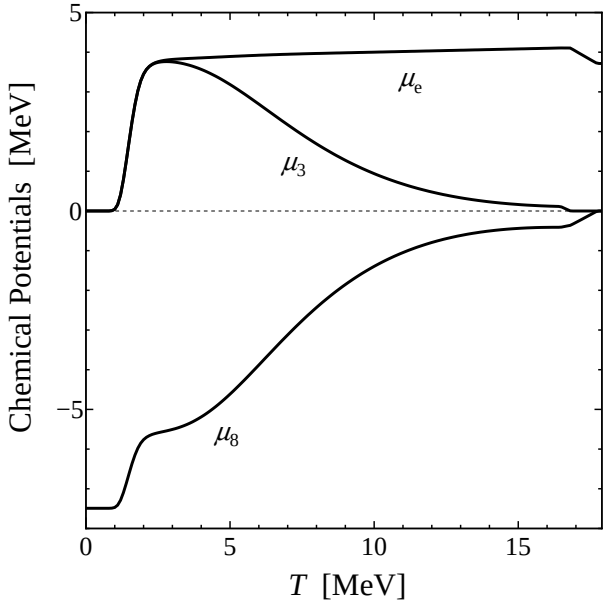

FIG. 11: Chemical potentials as a function of T at $M_s^2/\mu = 15$ MeV.

esting changes already at this relatively small temperature. The CFL→gCFL transition seen at zero temperature in Figs. 2 and 3 has become completely smooth at $T = 2$ MeV: there is no sharp difference between CFL and gCFL at nonzero T. Furthermore, note that the zero temperature transition from 2SC to g2SC is also washed out. This makes sense: at $T = 2$ MeV, it makes no physical difference whether a certain fermionic quasiparticle is gapless or has a gap that is nonzero but smaller than 2 MeV. So, although in Fig. 1 we have shown the values of M_s^2/μ where quark quasiparticles become gapless within the CFL, uSC and 2SC phases, these dashed lines have physical significance only where they intersect $T = 0$.

We see in Fig. 8 that Δ_1 vanishes at a second order CFL→uSC transition at $M_s^2/\mu = 85.1$ MeV. Another way to say this is that for $M_s^2/\mu < 85.1$ MeV, the critical temperature at which Δ_1 vanishes upon heating must be greater than 2 MeV, whereas for $M_s^2/\mu > 85.1$ MeV, this critical temperature is less than 2 MeV. As at $T = 0$, there is a first order phase transition, denoted in Fig. 8 by a thin vertical line, but here it is a first order phase transition between the uSC phase at $M_s^2/\mu < 125$ MeV and the 2SC phase at $M_s^2/\mu > 125$ MeV. The 2SC phase ends at a second order phase transition where $\Delta_3 \to 0$ at $M_s^2/\mu = 129$ MeV. This means that there is a regime of M_s^2/μ at which there is 2SC pairing at $T = 2$ MeV, but no pairing at $T = 0$. We investigate this further below.

We see in Fig. 9 that at small M_s^2/μ, the chemical potentials μ_e and μ_3 are both close to $M_s^2/4\mu$ at $T = 2$ MeV. This is qualitatively different than their zero temperature behavior $\mu_e = \mu_3 = 0$. In comparison, μ_e takes on the value $M_s^2/4\mu$ in unpaired quark matter. Thus, already at a temperature of only 2 MeV there is no sense in which μ_e is small. We see that at larger M_s^2/μ, μ_e and μ_3 diverge as at zero temperature, but they do so smoothly and they diverge from $M_s^2/4\mu$, rather than from 0. Since we have found that the CFL phase has become a metal already at $T = 2$ MeV, it is natural to ask at what temperature the insulator-metal crossover occurs. We answer this question at $M_s^2/\mu = 15$ MeV in Figs. 10 and 11. The latter figure shows a rapid insulator to metal crossover occurring between $T = 1$ MeV and $T = 2$ MeV, with μ_e, μ_3 and μ_8 all changing. We

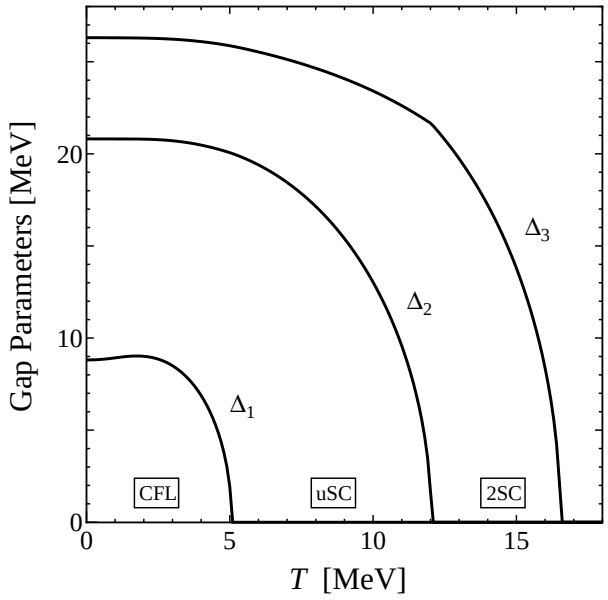

FIG. 12: Gap parameters versus temperature at $M_s^2/\mu = 70$ MeV.

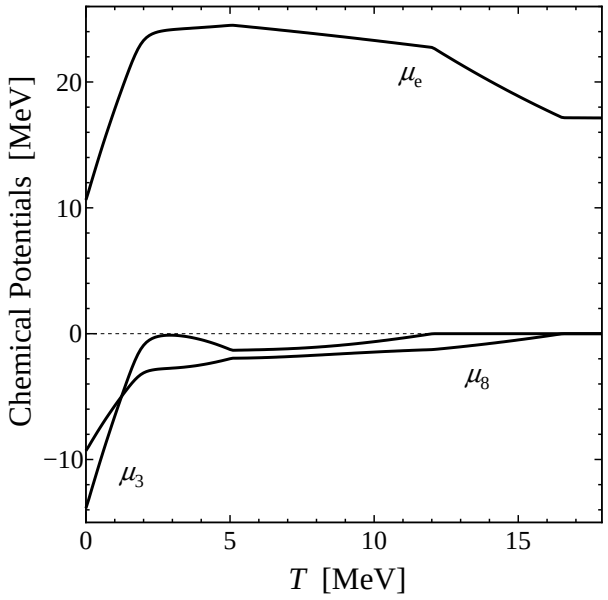

FIG. 13: Chemical potentials versus temperature at $M_s^2/\mu = 70$ MeV.

shall discuss this crossover at length in Section V. It can be understood analytically, and we shall see in Section V that the reason that μ_e takes on the value $M_s^2/4\mu$ is quite different from that in unpaired quark matter. Above the crossover, μ_e changes little as T increases further but both μ_3 and μ_8 decrease in magnitude. This occurs because at larger temperatures the gap parameters decrease, as seen in Fig. 10, and as the gap parameters vanish color neutrality occurs with $\mu_3 = \mu_8 = 0$ [16] whereas electrical neutrality still requires a nonzero μ_e.

We see in Fig. 10 that the gap parameters change little at the low temperatures at which the CFL phase is undergoing its insulator to metal crossover. Although it is not really visible in the figure, we find that $\Delta_2 > \Delta_1$ for $0 < T < 6.28$ MeV, and $\Delta_1 > \Delta_2$ at higher temperatures. At $T = 16.46$ MeV, Δ_2 vanishes at a second order phase transition and we find the dSC phase. Then, at $T = 16.81$ MeV, Δ_1 vanishes, yielding the 2SC phase. The final phase transition, at which Δ_3 vanishes, occurs at $T = 17.73$ MeV. This ordering of phase transitions is in qualitative agreement with that found in Ref. [16] using a Ginzburg-Landau approximation, and is in disagreement with the results of Ref. [15], in which no dSC regime was found. In order to gain confidence in the accuracy of our calculation and in the existence of the dSC phase, in Section VI we make a detailed and quantitative comparison between our results and those obtained via the Ginzburg-Landau approximation.

At larger values of M_s^2/μ, the ordering of phase transitions as a function of increasing temperature changes. For example, if we consider $M_s^2/\mu = 70$ MeV, in the gCFL phase at $T = 0$ with $\Delta_1 < \Delta_2 < \Delta_3$, we see in Fig. 12 that as the temperature is increased, Δ_1 vanishes first, then Δ_2 and then Δ_3, meaning that the phase which intervenes between CFL and 2SC is uSC, not dSC. This order of phase transitions is unsurprising, given that $\Delta_1 < \Delta_2 < \Delta_3$ at $T = 0$ in the gCFL phase. All three transitions are second order transitions in mean field theory. Fig. 13 shows the chemical potentials as a function of increasing temperature at $M_s^2/\mu = 70$ MeV. Whereas the $T = 0$ CFL phase undergoes an insulator to metal crossover as it is heated, the gCFL phase is already a metal at $T = 0$.

In both Figs. 10 and 12, we see a sequence of three second order phase transitions. The first of these, a transition from the CFL phase to either the dSC or the uSC phase, is likely not significantly affected by gauge field fluctuations, because the same gauge symmetries are unbroken (the $U(1)_{\tilde{Q}}$ symmetry) and broken (the other eight gauge symmetries) on both sides of the transition. It is therefore an interesting question for future work to consider the order parameter fluctuations at this transition, asking whether they render it first order or, if not, determining its universality class. The two mean field transitions occurring at higher temperatures in Figs. 10 and 12 will be qualitatively affected by gauge field fluctuations, as at each of them there are gauge symmetries that are broken on the low temperature side of the transition and restored above the transition. Gauge field fluctuations will presumably make these transitions first order, and shift their critical temperatures upward. These effects will be significant, because the relevant gauge fields are strongly coupled [9, 10].

We have found that at small M_s^2/μ, Δ_2 vanishes at a lower temperature than Δ_1 whereas at larger M_s^2/μ, these two transitions occur in the opposite order. There must, therefore, be some M_s^2/μ at which both vanish at the same temperature. We see in Fig. 1 that this "doubly

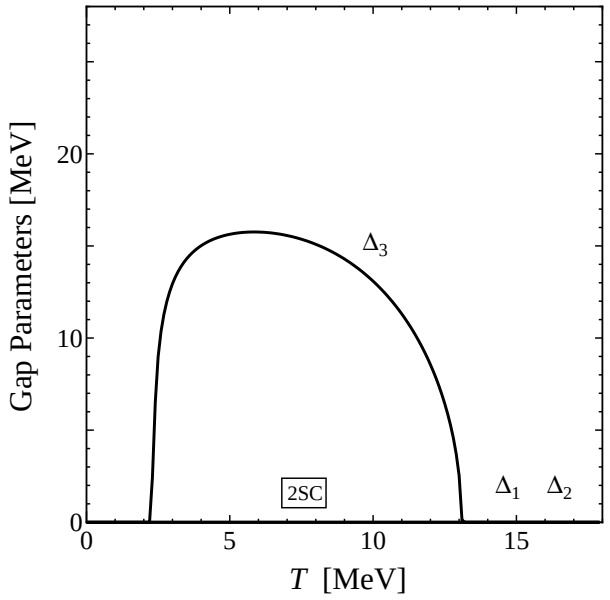

FIG. 14: Gap parameters versus temperature at $M_s^2/\mu = 130$ MeV. At this large value of M_s^2/μ, both Δ_1 and Δ_2 are zero at all temperatures. $\Delta_3 = 0$ at $T = 0$, but this gap parameter is nonzero for 2.37 MeV $< T <$ 13.08 MeV.

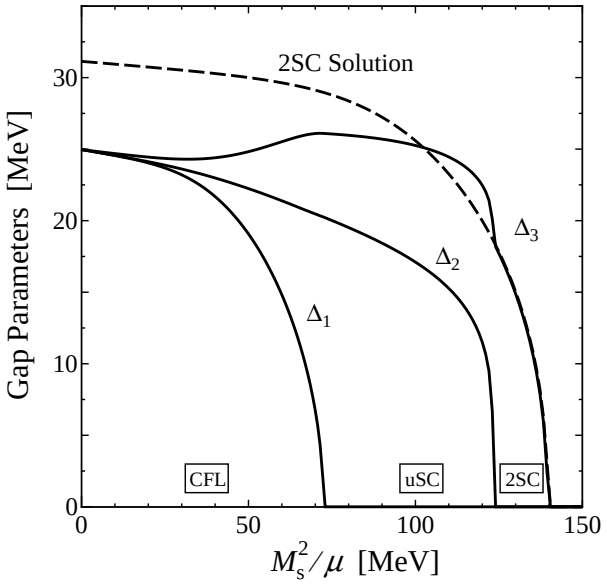

FIG. 15: Gap parameters versus M_s^2/μ at $T = 4$ MeV.

critical" point occurs at $T = 15.3$ MeV and $M_s^2/\mu = 29.4$ MeV.

Having followed what happens upon heating the CFL phase at $M_s^2/\mu = 15$ MeV and upon heating the gCFL phase at $M_s^2/\mu = 70$ MeV, in Fig. 14 we consider heating quark matter at $M_s^2/\mu = 130$ MeV, which is unpaired at $T = 0$. We see that Δ_3 becomes nonzero at a second order phase transition, and then vanishes at a higher temperature at a second second order phase transition. This behavior has been described previously [35, 40], and can be understood as follows. At $T = 0$, the u and d Fermi surfaces in the unpaired quark matter are too far apart to allow 2SC pairing. However, as we increase T, we excite u quarks above the u Fermi surface, and d holes below the d Fermi surface. This smearing of the separated Fermi surfaces assists u-d pairing, and Δ_3 turns on at a nonzero temperature. Of course, at a still higher temperature the Δ_3 condensate melts.

The final slice of the phase diagram of Fig. 1 that we shall show explicitly is a plot of the gap parameters as a function of M_s^2/μ at $T = 4$ MeV, shown in Fig. 15. By comparing this figure with Fig. 8, we see qualitative changes in the physics between $T = 2$ MeV and $T = 4$ MeV: the 2SC phase now takes over from the uSC phase not via a first order phase transition, but instead via a second order phase transition at $M_s^2/\mu = 123.2$ MeV at which $\Delta_2 \to 0$. This means that a line of first order phase transitions, present at lower temperatures, has turned into a second order transition at a tricritical point. This tricritical point is shown by a diamond in Fig. 1, and is located between $T = 3.9$ MeV and $T = 4.0$ MeV.

The results that we have presented up to this point in this section, plotted in Figs. 8 through 15, constitute a description of all of the features at $T \neq 0$ depicted in the phase diagram given in Fig. 1. We now ask how this phase diagram changes as we vary the strength of the interaction, and hence Δ_0. If we reduce Δ_0, there are no qualitative changes as long as we rescale the vertical and horizontal axes of the phase diagram by the same factor that we reduce Δ_0. As at $T = 0$, however, increasing Δ_0 leads to qualitative changes in the phase diagram at large M_s^2/μ, indicating that the details of the large M_s^2/μ regions of the phase diagram are not robust predictions of our model.

With $\Delta_0 = 40$ MeV, in Fig. 16, we see the same three special points as in Fig. 1: a quantum critical point separating the CFL and gCFL phases at $T = 0$, a doubly critical point at which the $\Delta_1 \to 0$ and $\Delta_2 \to 0$ transitions cross, and a tricritical point at large M_s^2/μ at which a line of first order phase transitions ends. Since both axes of Fig. 16 have been rescaled by 40/25 relative to Fig. 1, the two figures are qualitatively similar: the one qualitative change occurs at large M_s^2/μ, where the g2SC phase extends down to $T = 0$, as we have already seen in Fig. 5. (At $T = 0$, there is a sharp distinction between 2SC and g2SC, and in this instance the phase is g2SC.) The most interesting quantitative change is a change in the slopes of the $\Delta_1 \to 0$ and $\Delta_2 \to 0$ transitions on the phase diagram at small M_s^2/μ, which pushes the doubly critical point somewhat down in temperature. This effect is more clearly visible at stronger coupling, with $\Delta_0 = 100$ MeV, as shown in Fig. 17. We shall explain this quantitatively in Section VI.

With $\Delta_0 = 100$ MeV, in Fig. 17, we see further qualitative changes at large M_s^2/μ, corresponding to those at $T = 0$ shown in Fig. 6. Now, the uSC phase and

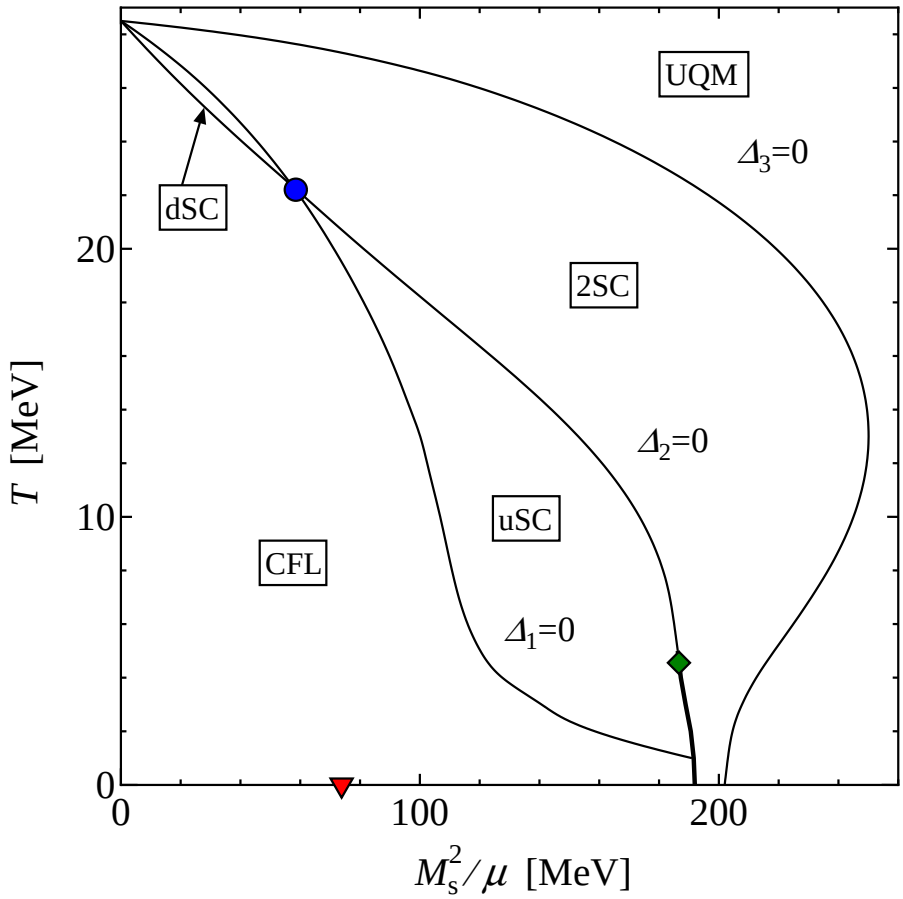

FIG. 16: Phase diagram of dense neutral quark matter in the $(M_s^2/\mu, T)$ plane, with a coupling chosen such that $\Delta_0 = 40$ MeV. (All parameters except Δ_0 are the same as in Fig. 1.) Only phase transitions are shown — the analogues of the dashed and dotted lines in Fig 1 are not given.

the 2SC phase both extend to $T = 0$. And, at $T = 0$ there is a 2SC regime separated from g2SC by a quantum critical point, like that separating the CFL and gCFL phases at $T = 0$. If we start at $T = 0$ in the g2SC phase and heat the system, Δ_3 at first increases, before decreasing at higher temperature, eventually vanishing at the upper phase transition shown in Fig. 17. If we extended the phase diagram to $M_s^2/\mu \to \infty$, this critical temperature would become M_s-independent in the limit. The small remaining M_s-dependence at the largest M_s^2/μ we show is easily understood: even though there are no strange quarks present at $T = 0$ at these large values of M_s, meaning that the $T = 0$ physics has become M_s-independent, strange quarks can still be excited at nonzero temperature.

As Δ_0 is increased from 40 MeV to 100 MeV, the phase diagram changes continuously from that of Fig. 16 to that of Fig. 17. First, the uSC phase reaches the $T = 0$ axis. Next, the tricritical point indicated by the diamond in Fig. 16 retreats down to $T = 0$. All the while, the (g)2SC region is extending farther and farther to the right, eventually to $M_s \to \infty$ when the coupling is strong enough to allow ud pairing even once there are no strange quarks present.

We shall discuss the implications of the phase diagrams that we have found in Section VII. First, however, our investigation has raised several interesting questions that we have been able to address analytically, as we describe in Sections V and VI.

V. HEATING THE CFL PHASE: UNDERSTANDING THE INSULATOR TO METAL CROSSOVER

We have seen in Fig. 11 that as CFL quark matter is heated, it undergoes a crossover from an insulator, with μ_e exponentially small, to a metal, with $\mu_e \sim M_s^2/4\mu$. With $\Delta_0 = 25$ MeV and $M_s^2/\mu = 15$ MeV as in Fig. 11, the crossover occurs between $T = 1$ MeV and $T = 2$ MeV. This insulator to metal crossover has been seen previously in Ref. [15]; our goal here is to understand it analytically.

We see from Fig. 10 that the gap parameters change little between $T = 1$ MeV and $T = 2$ MeV, whereas the chemical potentials change dramatically. We shall

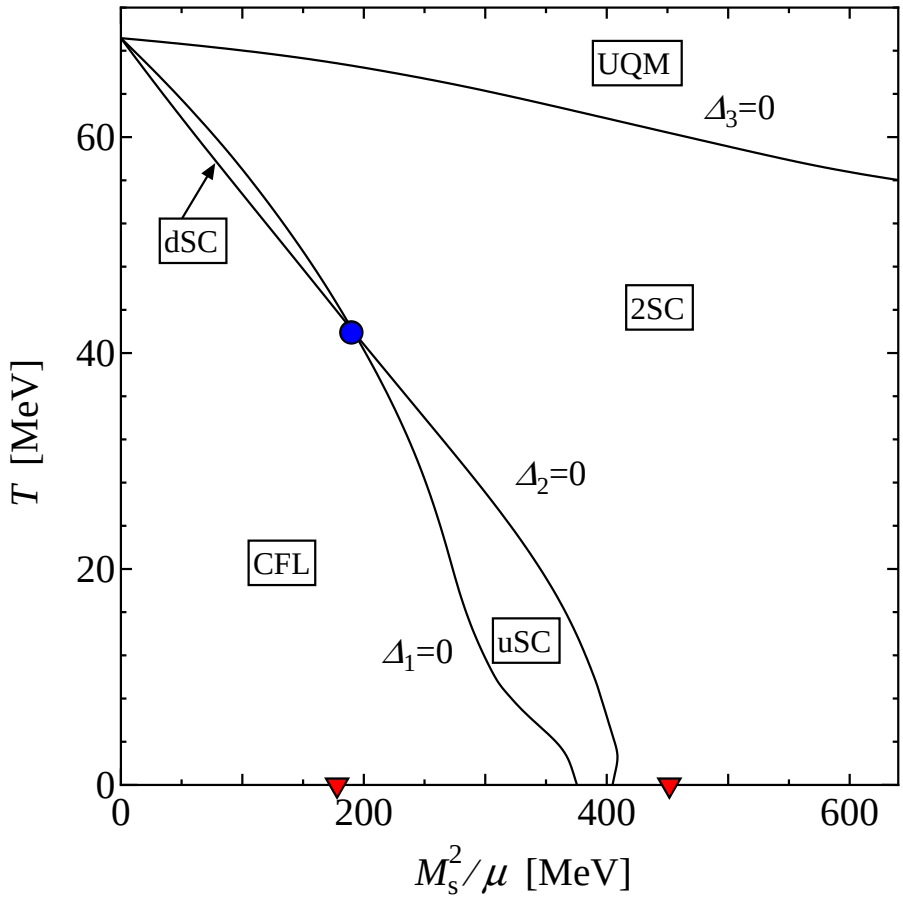

FIG. 17: Phase diagram of dense neutral quark matter in the $(M_s^2/\mu, T)$ plane, with a coupling chosen such that $\Delta_0 = 100$ MeV. (All parameters except Δ_0 are the same as in Figs. 1 and 16.) The two triangles on the $T = 0$ axis indicate quantum critical points at which modes become gapless. The first, which separates the CFL and gCFL phases, is familiar. The second separates 2SC and g2SC phases, as shown in Fig. 6.

explain the variation of the chemical potentials, treating the gap parameters as T-independent. We note from Fig. 11 that during the crossover, μ_e increases from near 0 to near $M_s^2/4\mu$, while μ_3 increases by the same amount and μ_8 increases by half as much. This tells us that (7) and (8) are maintained, and hence it is the combination $\mu_{\tilde{Q}}$ of (6) that is changing. We recall that at $T = 0$ the contribution of the quark matter to the free energy Ω is independent of $\mu_{\tilde{Q}}$, and this "plateau" is only curved by the small contribution of the electrons to the free energy, of order μ_e^4, which favors $\mu_e = 0$. Above the crossover we find $\mu_e \simeq M_s^2/4\mu$, which is on the plateau but away from the point on the plateau favored by the electron neutrality condition. In order to understand the crossover, then, there must be thermally excited $\tilde{Q}$-charged quasiparticles whose neutrality condition favors $\mu_e \neq 0$, and we must see the curvature of the free energy plateau due to these quasiparticles "take over" from that due to the electrons. We first show that the CFL quark quasiparticle excitations have the desired effect, and then in Section V A we show that the thermally excited charged mesonic pseudo-Nambu-Goldstone boson excitations of the CFL phase play a negligible role.

The quarks with nonzero $\tilde{Q}$ are the rs and bu which pair with gap parameter Δ_2, and the rd and gu which pair with gap parameter Δ_3. This means that in the CFL phase there are two quasiquarks with $\tilde{Q} = +1$ (one a linear combination of bu quarks and rs holes; the other a linear combination of gu quarks and rd holes) and two quasiquarks with $\tilde{Q} = -1$ (one a linear combination of rs quarks and bu holes; the other a linear combination of rd quarks and gu holes).

We now evaluate the dispersion relations of these excitations, and estimate the number density of thermally excited charged quasiquarks. In this Section, we shall follow Refs. [5, 6] and include the nonzero strange quark mass only via its effect as a shift in the chemical potentials of the strange quarks. We have seen in Section III that this is a good approximation in the CFL phase. The dispersion relations of these four quasiparticles are given

by [6]

$$\varepsilon_{(rs\text{-}bu)}(p) = \pm\tfrac{1}{2}\left(\mu_{rs} - \frac{M_s^2}{2\mu} - \mu_{bu}\right) + \sqrt{\left(p - \bar{\mu}_{(bu\text{-}rs)} + \frac{M_s^2}{4\mu}\right)^2 + \Delta_2^2}$$
$$\varepsilon_{(rd\text{-}gu)}(p) = \pm\tfrac{1}{2}(\mu_{gu} - \mu_{rd}) + \sqrt{(p - \bar{\mu}_{(rd\text{-}gu)})^2 + \Delta_3^2} \tag{22}$$

where $\bar{\mu}_{bu\text{-}rs} \equiv (\mu_{bu} + \mu_{rs})/2$ and $\bar{\mu}_{rd\text{-}gu} \equiv (\mu_{rd} + \mu_{gu})/2$. Upon substituting the definitions (19) and the relations (7) and (8), which are maintained through the crossover, these become

$$\varepsilon_{(rs\text{-}bu)}(p) = \pm\left(\mu_e - \frac{M_s^2}{2\mu}\right) + \sqrt{\left(p - \mu + \frac{M_s^2}{6\mu}\right)^2 + \Delta_2^2}$$
$$\varepsilon_{(rd\text{-}gu)}(p) = \pm\mu_e + \sqrt{\left(p - \mu + \frac{M_s^2}{6\mu}\right)^2 + \Delta_3^2}\ . \tag{23}$$

At the temperatures of interest, these excitation energies are all greater than T, and so only the lowest energy excitation with each $\tilde{Q}$ charge matters — the number density of the higher energy excitations is exponentially smaller. Labeling the quasiparticles by their $\tilde{Q}$ charge, the excitation energies of the lowest lying charged quasiquarks are

$$\varepsilon_{+1}(p) = \left(\mu_e - \frac{M_s^2}{2\mu}\right) + \sqrt{\left(p - \mu + \frac{M_s^2}{6\mu}\right)^2 + \Delta_2^2}$$
$$\varepsilon_{-1}(p) = -\mu_e + \sqrt{\left(p - \mu + \frac{M_s^2}{6\mu}\right)^2 + \Delta_3^2}\ , \tag{24}$$

corresponding to the $(rs\text{-}bu)$ quasiquark with $\tilde{Q} = +1$ and the $(rd\text{-}gu)$ quasiquark with $\tilde{Q} = -1$. We now evaluate the T-dependent contribution of these quasiquarks to the free energy Ω given by (13). Because the quasiquark energies are much larger than the temperatures of interest, the Boltzmann factors are small, the integral is dominated by p near the minimum of $\varepsilon(p)$, and we can use the saddle-point approximation. We find that, for example, the contribution of the $\tilde{Q} = +1$ quasiquark to Ω is given by

$$\begin{aligned} &-\frac{1}{\pi^2}\int_0^\Lambda dp\, p^2 T \ln\bigl(1 + \mathrm{e}^{-|\varepsilon_{+1}(p)|/T}\bigr) \\ &\simeq -\frac{1}{\pi^2}\int_0^\Lambda dp\, p^2 T\, e^{-|\varepsilon_{+1}(p)|/T} \\ &\simeq -\frac{1}{\pi^2}\sqrt{2\pi\Delta T}\bar{\mu}^2 T e^{-|\varepsilon_{+1}(\bar{\mu})|/T}\ , \end{aligned} \tag{25}$$

where $\bar{\mu} \equiv \mu - M_s^2/6\mu$. The contribution of the $\tilde{Q} = -1$ quasiparticle is analogous. The contribution of these two quasiparticles to the $\tilde{Q}$-charge density is then

$$(\tilde{Q} = +1) \qquad \frac{\sqrt{2\pi\Delta T}\bar{\mu}^2}{\pi^2} e^{-(\Delta + \mu_e - M_s^2/2\mu)/T}, \tag{26}$$
$$(\tilde{Q} = -1) \qquad -\frac{\sqrt{2\pi\Delta T}\bar{\mu}^2}{\pi^2} e^{-(\Delta - \mu_e)/T}. \tag{27}$$

We have set $\Delta_3 = \Delta_2 \equiv \Delta$, a good approximation throughout the crossover as shown in Fig. 10. $\tilde{Q}$-neutrality is a balance between the charge densities of these two quark quasiparticles and the electrons.

We can now see that what drives the system to $\mu_e \neq 0$ is the fact that the lightest $\tilde{Q} = +1$ and $\tilde{Q} = -1$ quark quasiparticles have dispersion relations with different gaps when $M_s \neq 0$, and consequently contribute charge densities of different magnitudes when thermally excited. If we attempt to set $\mu_e = 0$ at $T \neq 0$, there are more $\tilde{Q} = +1$ quasiparticles present than $\tilde{Q} = -1$ quasiparticles, and the system is not neutral. To achieve neutrality, μ_e must be increased as this increases the density of $\tilde{Q} = -1$ quasiparticles, decreases the density of $\tilde{Q} = +1$ quasiparticles, and adds electrons, which have $\tilde{Q} = -1$. This is described by the neutrality condition

$$\frac{2\sqrt{2\pi\Delta T}\bar{\mu}^2}{\pi^2}\mathrm{e}^{-(\Delta - M_s^2/4\mu)/T}\sinh\left(\frac{M_s^2/4\mu - \mu_e}{T}\right) - \frac{\mu_e^3}{3\pi^2} - \frac{\mu_e T^2}{3} = 0\ , \tag{28}$$

which we can solve for $\mu_e(T)$ if we take Δ to be T-independent.

Let us now investigate the implications of this result. At very small T, the quark quasiparticles are exponentially rare, and those with $\tilde{Q} = -1$ are exponentially rarer than those with $\tilde{Q} = +1$. The $\tilde{Q} = +1$ quasiparticle density is balanced by the electron density, and μ_e is exponentially small. However, the quasiparticle densities are proportional to μ^2 whereas the electron density is not. This means that at the T at which μ_e starts to take off, the quasiparticle Boltzmann factors are still rather small. Once T is large enough that μ_e approaches $M_s^2/4\mu$, however, even though the individual Boltzmann factors continue to rise rapidly as T increases further, the sinh factor in (28) becomes small. Neutrality at this point is primarily a balance between the densities of the $\tilde{Q} = +1$ and $\tilde{Q} = -1$ quasiparticles, with electrons cancelling only the small difference between their densities. The result, seen already in Fig. 11 and shown in greater detail in Fig. 18 is a crossover in which μ_e is at first exponentially small, then rises rapidly, and then saturates as it approaches $M_s^2/4\mu$. We see in Fig. 18 that the equation (28 for μ_e that we have derived , making approximations as described, gives a very good description of the numerical solution of the full coupled gap and neutrality equations. This demonstrates that (28) provides us with a good analytic description of the insulator to metal crossover that CFL quark matter experiences when heated.

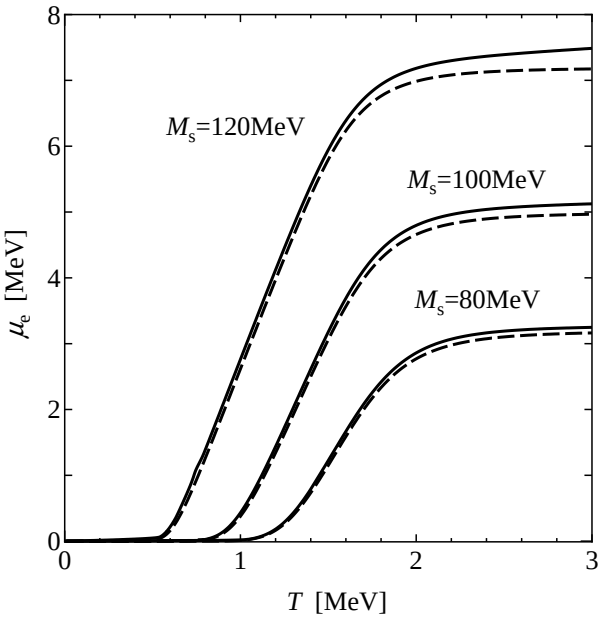

FIG. 18: Comparison between the analytic results (dashed curves) and the numerical results (solid curves) for μ_e as a function of temperature with $\Delta_0 = 25$ MeV for several values of M_s in the CFL phase. The analytic results were obtained from (28), and the numerical results were obtained by solving the full coupled gap equations and neutrality conditions, as in previous Sections. In evaluating μ_e from (28) we have taken Δ to be the average of Δ_2 and Δ_3 at the midpoint of the crossover.

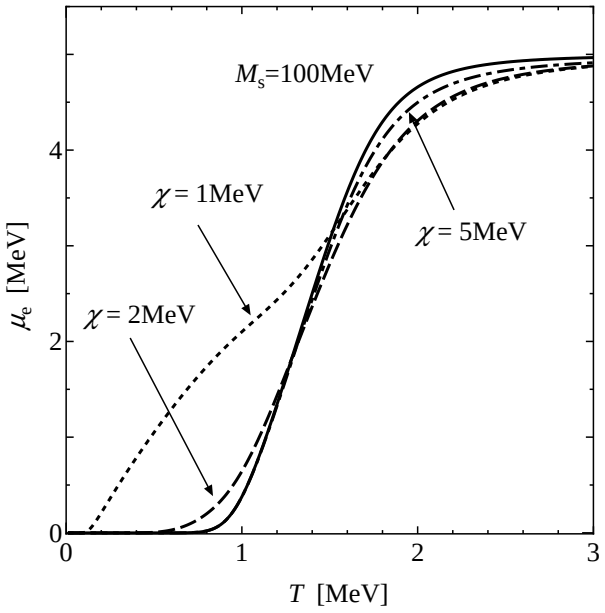

FIG. 19: Comparison between the analytic estimate for μ_e versus T with and without charged meson contributions. The solid curve, with no meson contributions, is the same as the $M_s = 100$ MeV analytic estimate in Fig. 18. The dashed curves include the contribution of thermally excited charged pions and kaons, for three values of the parameter χ described in the text that parameterizes the instanton contribution to the meson masses.

We have set the electron mass to zero in Fig. 18 and throughout. Including it means that it takes a larger μ_e to achieve a given electron density, pushing all the curves in Fig. 18 very slightly upwards. With an electron mass as in nature, the effect on the curves is invisible on the scale of the plot.

A. Contribution of charged mesons

As described in Section II B, there are other charged excitations in the CFL phase. Among the pseudo-Nambu-Goldstone bosons, there are mesons with the quantum numbers of the $\pi^\pm$ and $K^\pm$. We have neglected the contribution of thermally excited charged mesons to the charge density in the derivation of (28). We now investigate this approximation.

The dispersion relations of the charged mesons, together with that for the K^0-meson which we shall also need below, are given by [12, 23, 24, 25, 26, 27]

$$\begin{aligned}
\varepsilon_{\pi^\pm}(p) &= \pm\mu_e + \sqrt{v^2p^2 + M^2_{\pi^\pm}} \\
\varepsilon_{K^\pm}(p) &= \pm\mu_e \mp \frac{M_s^2}{2\mu} + \sqrt{v^2p^2 + M^2_{K^\pm}} \\
\varepsilon_{K^0}(p) &= -\frac{M_s^2}{2\mu} + \sqrt{v^2p^2 + M^2_{K^0}}\ ,
\end{aligned} \tag{29}$$

where $v^2 = 1/3$ at high density [25]. The meson masses in the CFL phase are given by

$$\begin{aligned}
M^2_{\pi^\pm} &= a(M_u + M_d)M_s + \chi(M_u + M_d) \\
M^2_{K^\pm} &= a(M_u + M_s)M_d + \chi(M_u + M_s) \\
M^2_{K^0} &= a(M_d + M_s)M_u + \chi(M_d + M_s)\ .
\end{aligned} \tag{30}$$

Here, $a = 3\Delta^2/\pi^2 f_\pi^2$ with $f_\pi^2 = (21 - 8\log 2)\mu^2/36\pi^2$ at high density [25], which yields $a = 0.0175$ for $\Delta_0 = 25$ MeV at $\mu = 500$ MeV. And, χ parameterizes the contribution of $U(1)_A$-breaking instanton effects which generate $\langle\bar{q}q\rangle$ condensates and therefore contributions to meson masses in the CFL phase [23, 24, 27], via the 't Hooft interaction which contributes couplings of the form $\Delta^2\langle\bar{q}q\rangle$. The magnitude of χ is not well known, as it depends on the instanton size distribution and instanton form factors at nonzero density. It has been estimated to lie in the range 1 MeV $< \chi <$ 100 MeV [24, 27]. In Fig. 19, we include the contribution of all four charged

mesons to the $\tilde{Q}$-charge neutrality condition, determining the density of thermally excited bosonic quasiparticles from the dispersion relations. The contribution to the charge density from the $K^{\pm}$ mesons is

$$\frac{1}{2\pi^2}\int_0^\infty dp\, p^2\left(\frac{1}{\exp\left[\varepsilon_{K^+}(p)/T\right]-1}-\frac{1}{\exp\left[\varepsilon_{K^-}(p)/T\right]-1}\right), \tag{31}$$

and that from the pions is analogous. We then solve for μ_e vs. T, taking $M_s = 100$ MeV and $M_u = 5$ MeV and $M_d = 10$ MeV. We plot the results for $\chi = 1$, 2 and 5 MeV in Fig. 19.

Adding the charged mesons adds new charge carriers, and so the simplest expectation for their effects is that a smaller μ_e will be required in order to neutralize the imbalance in the fermionic quasiparticle sector. We see in Fig. 19 that this expectation is borne out above the crossover, but not below. Above the crossover, we see that μ_e is reduced relative to the results we obtained in Fig. 18, where we neglected the mesons. The mesonic contributions get less significant at larger values of χ, as the mesons get heavier. They are already small for $\chi = 1$ MeV and are negligible by $\chi = 5$ MeV. At low temperatures, and for the smallest values of χ, there is another effect to be understood. The dispersion relations for the $K^{\pm}$ in (29) indicate that the K^+ is easier to excite than the K^-. This means that they behave like the quasiquarks, in the sense that at a nonzero temperature they contribute a positive $\tilde{Q}$-charge density, which must be cancelled. If χ is very small, the K^+ charge density becomes significant at such a low temperature that its contribution can only be cancelled by electrons — the Boltzmann factors for all other excitations are still prohibitive. This means that if χ is very small, μ_e initially rises with temperature significantly more rapidly than in the absence of the mesons. We see this effect clearly in Fig. 19 for $\chi = 1$ MeV and still to a small degree for $\chi = 2$ MeV. For $\chi = 5$ MeV, $\mu_e(T)$ is indistinguishable at low temperatures from that in the absence of the mesons.

We can summarize the results in Fig. 19 as follows. For $\chi \gtrsim 2$ MeV, the thermally excited charged mesons have no significant effects at any temperature. But, if $\chi \sim 1$ MeV, which is at the bottom end of the estimated allowed range 1 MeV $< \chi <$ 100 MeV [24, 27], the K^+ excitations contribute significantly at very low temperatures.

At much larger temperatures, well above the insulator to metal crossover that we have analyzed, we come to the various critical temperatures that we have seen in Section IV and will analyze further in Section VI. At these temperatures, at which gap parameters vanish, it is well understood that the fermionic quasiparticles are the most important degrees of freedom. What we have shown is that at low temperatures also, the charged mesons are less important than the charged fermions among the thermal excitations, as long as χ is not very small.

Mesons can nevertheless play an important role if they condense [12]. At $T = 0$, the CFL phase is stable against meson condensation as long as $\varepsilon_{K^0} > 0$ at $p = 0$. (K^0-condensation yields the most stringent constraint.) This requires $M_{K^0}^2 > M_s^4/4\mu^2$, corresponding to $\chi \gtrsim M_s^3/4\mu^2$. For $M_s = 100$ MeV, as in Fig. 19, this requires $\chi > 1$ MeV. We are therefore justified in our neglect of K^0-condensation in Fig. 19. If $\chi > 3.6$ MeV, there is no K^0-condensation in the CFL phase with $\Delta_0 = 25$ MeV for $M_s^2/\mu < 46.8$ MeV, meaning that there is no K^0-condensation at $T = 0$ for all values of M_s^2/μ below the CFL→gCFL transition. (K^0-condensation in the gCFL phase has yet to be analyzed.) It seems likely that $\chi > 3.6$ MeV at accessible densities, since χ is larger at lower densities and the analysis in Ref. [24] which yields the estimate 1 MeV $< \chi <$ 100 MeV becomes more reliable at higher densities. If the coupling is stronger, however, K^0-condensation becomes more likely. For example, for $\Delta_0 = 100$ MeV, there is no K^0-condensation in the CFL phase only if $\chi > 26$ MeV. If K^0-condensation were to occur, it delays the CFL→gCFL transition, increasing the M_s^2 at which it occurs by a factor 4/3 if $\chi = 0$ [13]. Further work remains to be done, for example extending the analysis of Ref. [13] to nonzero χ and to the gCFL phase.

Another issue that remains to be investigated is the possibility of π^- condensation at nonzero temperature. We have seen that above the insulator to metal transition, $\mu_e \approx M_s^2/4\mu$. At zero temperature, this would lead to π^- condensation if $\chi < M_s^4/(16\mu^2(M_u+M_d))$, but this μ_e only arises at $T \neq 0$, and nonzero T acts to stabilize against meson condensation.

Finally, all these issues should be investigated in an expanded model in which the 't Hooft interaction is included from the beginning in the free energy and hence in the gap and neutrality conditions, and the quark masses are also solved for dynamically.

VI. THE GINZBURG-LANDAU APPROXIMATION

In the $M_s^2/\mu \to 0$ limit, the three critical temperatures at which the gap parameters vanish become one. Near this critical temperature, where all gap parameters are small, a Ginzburg-Landau approximation can be employed. The Ginzburg-Landau free energy was analyzed at $M_s = 0$ in Refs. [3, 17], and was extended to small but nonzero M_s^2/μ in Ref. [16]. We wish to compare our results at small but nonzero M_s^2/μ to those obtained in the Ginzburg-Landau approximation, and to compare the coefficients in the Ginzburg-Landau potential (actually, ratios of coefficients) in our model to those calculated in QCD at asymptotic densities and thus at weak coupling in Refs. [3, 16].

The Ginzburg-Landau potential is parameterized

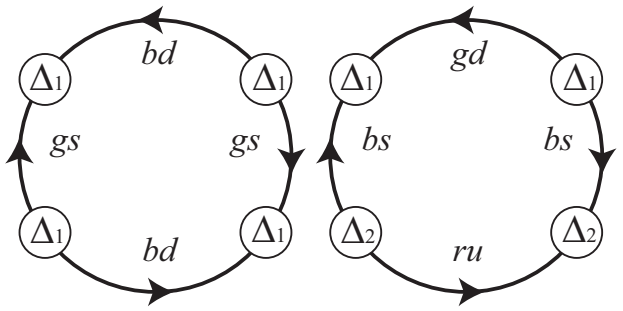

FIG. 20: Diagrams contributing to the Δ_1^4 and $\Delta_1^2\Delta_2^2$ terms in the Ginzburg Landau potential (32).

as [16]

$$\begin{aligned}\Omega =&\alpha\left(\Delta_1^2+\Delta_2^2+\Delta_3^2\right)\\ &+\epsilon\left(\Delta_1^2+\Delta_2^2\right)+\tfrac{1}{3}\eta\left(-2\Delta_1^2+\Delta_2^2+\Delta_3^2\right)\\ &+\beta_1\left(\Delta_1^2+\Delta_2^2+\Delta_3^2\right)^2+\beta_2\left(\Delta_1^4+\Delta_2^4+\Delta_3^4\right),\end{aligned} \tag{32}$$

where $\alpha=\alpha_0(T-T_c)/T_c$ and where the coefficients ϵ and η are proportional to M_s^2 and μ_e respectively and are therefore present only if $M_s\neq 0$. The form of the ϵ and η terms was derived in Ref. [16] for QCD at asymptotic densities. In the Ginzburg-Landau limit, in which all gap parameters are small, color neutrality occurs with μ_3 and μ_8 vanishingly small [16], and electrical neutrality requires a nonzero μ_e, of order $M_s^2/4\mu$ as in unpaired quark matter. At low temperatures, the most important consequences of M_s and μ_e (and also μ_3 and μ_8) derive from the stress they put on pairing, as they (seek to) push Fermi momenta apart. Near T_c, $T\gg\Delta$. And, we are working at $M_s^2/\mu\ll T_c$, where the thermal smearing of the Fermi distributions is much greater than the splittings between Fermi momenta. In this regime, the effects of M_s^2 or μ_e on the pairing of two quarks do not arise from the splitting between their Fermi momenta, as this is negligible. The effects of M_s^2 or μ_e arise from the change in the *average* Fermi momenta of the two quarks, and hence in the density of states, that M_s^2 or μ_e induces. For example, M_s^2 depresses the average Fermi momenta of u-s and d-s pairs, but does not affect u-d pairs. This explains the form of the ϵ term in (32). On the other hand, $\mu_e>0$ increases the average Fermi momenta of d-s pairs, while decreasing that of u-d and u-s pairs. This explains the form of the η term.

In Ref. [3] it is shown that, in the weak coupling regime, $\beta_1=\beta_2$. This result is valid beyond weak coupling, however, as all that is required to demonstrate it is the pairing ansatz (3) and the mean field approximation. The quarks in the 2×2 blocks contribute through diagrams like the first in Fig. 20, leading to a contribution proportional to $\Delta_1^4+\Delta_2^4+\Delta_3^4$. The quarks in the 3×3 block contribute through diagrams like both the first and second in Fig. 20, leading to a contribution proportional to $\Delta_1^4+\Delta_2^4+\Delta_3^4+2\Delta_1^2\Delta_2^2+2\Delta_2^2\Delta_3^2+2\Delta_1^2\Delta_3^2$. Adding all the diagrams, we conclude that $\beta_1=\beta_2$.

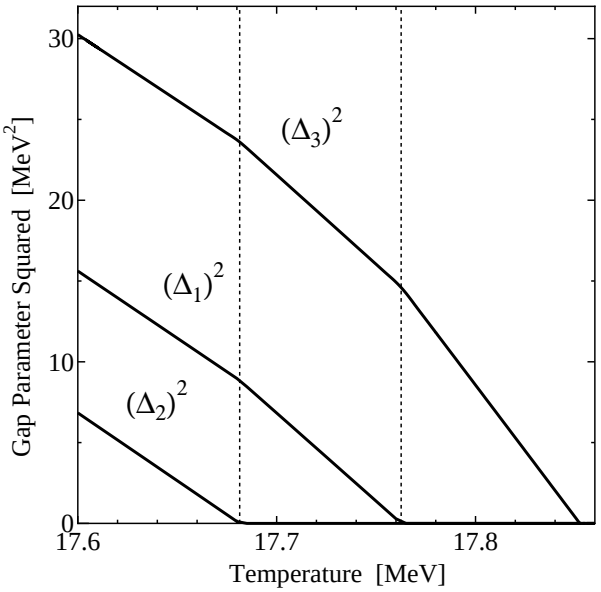

FIG. 21: Gap parameters squared versus T at $M_s=30$ MeV, namely $M_s^2/\mu=1.8$ MeV. This figure should be compared to the "schematic illustration" given in Fig. 2 of Ref. [16]. We see the three phase transitions separating the CFL, dSC, 2SC and unpaired phases.

We now wish to confirm that (32) correctly describes the M_s-dependent physics in our model. We do so by extracting the ratio

$$\zeta\equiv\frac{\epsilon}{\eta} \tag{33}$$

from our results in three independent ways. If (32) is correct — that is if there are no M_s-dependent terms missed — the three extractions of ζ should agree. We see in the phase diagrams of Figs. 1, 16 and 17 that the slopes of the three transition temperatures (i.e. $dT_c/d(M_s^2/\mu)$ at $M_s^2/\mu=0$) are different, with that for the $\Delta_3\to 0$ critical temperature the shallowest and that for the $\Delta_2\to 0$ critical temperature the steepest. The ratios of these slopes can be extracted from the Ginzburg-Landau free energy Ω of (32) and are given by

$$1:(6\zeta-5):(6\zeta+4) \tag{34}$$

where we have used $\beta_1=\beta_2$. We can also read the slopes directly from our phase diagrams. The $\Delta_0=25$ MeV phase diagram of Fig. 1 yields the ratios

$$1:10.1:19.1 \tag{35}$$

which can be used to obtain two independent extractions of ζ, one from $1:(6\zeta-5)=1:10.1$ and the other from $1:(6\zeta+4)=1:19.1$. The two are in perfect agreement, with both yielding $\zeta=2.52$ for $\Delta_0=25$ MeV.

A third extraction can be obtained from Fig. 21 upon realizing that, according to (32), in the CFL phase where

all three gap parameters are nonzero ζ is given by the ratio

$$\frac{\Delta_3^2 - \Delta_2^2}{\Delta_1^2 - \Delta_2^2} \ . \tag{36}$$

This ratio can be extracted at $M_s^2/\mu = 1.8$ MeV from Fig. 21. We have done this extraction at a number values of M_s^2/μ and fitted the results as

$$\frac{\Delta_3^2 - \Delta_2^2}{\Delta_1^2 - \Delta_2^2} = 2.52 + 36.2\left(\frac{M_s}{\mu}\right)^2 + 1.02\times 10^3\left(\frac{M_s}{\mu}\right)^4 \tag{37}$$

which leads us to conclude for the third time that $\zeta = 2.52$ for $\Delta_0 = 25$ MeV. In (37) we have extracted the M_s^2/μ^2 and M_s^4/μ^4 corrections to the ratio (36), in addition to extracting ζ. The coefficients we have obtained confirm that these higher order terms are negligible as long as $M_s^2/\mu^2 \ll T_c/\mu$ or, equivalently given (1), $M_s^2/\mu \ll \Delta_0$. This indicates yet again that the Ginzburg-Landau free energy (32) provides a good approximation to our results in the regime where it should be valid.

Upon comparing our Fig. 21 with the schematic illustration given in Fig. 2 of Ref. [16], there can already be little doubt that the Ginzburg-Landau potential (32) correctly describes the results that we have obtained by solving the full gap and neutrality equations numerically, for $T \sim T_c$ and for $M_s^2/\mu^2 \ll T_c/\mu$. The agreement between our three extractions of ζ makes this point quantitatively.

We can also use Fig. 21 to check that our numerical results are consistent with $\beta_1 = \beta_2$. The Ginzburg-Landau potential (32) can first be used to show that in the CFL (and dSC) phases in Fig. 21 the slopes of the lines for the three (two) nonzero gap parameters are the same. Our results clearly satisfy this. Next, the Ginzburg-Landau potential (32) can be used to show that the ratio of the slopes of the gap parameters in the CFL phase in Fig. 21 to those in the dSC phase is $(2\beta_1 + \beta_2)/(3\beta_1 + \beta_2)$, and the ratio of those in the dSC phase to that in the 2SC phase is $(\beta_1 + \beta_2)/(2\beta_1 + \beta_2)$. These ratios cannot be extracted very accurately from Fig. 21, given the narrow windows within which the dSC and 2SC phases are found. However, they are consistent with 3/4 and 2/3, corresponding to $\beta_1 = \beta_2$.

In Ref. [16], the ratio ζ is calculated using weak coupling methods, valid at asymptotic densities. The weak coupling result is $\zeta = 2$. From our numerical results, we have found $\zeta = 2.52$ at $\Delta_0 = 25$ MeV. We also find $\zeta = 2.69$ at $\Delta_0 = 40$ MeV and $\zeta = 3.87$ at $\Delta_0 = 100$ MeV, extracting ζ from the ratio (36) as in (37). At weak coupling, $\zeta = 2$ and the Δ_3^2 and Δ_2^2 lines are equidistant from the Δ_1^2 line in the CFL phase region of Fig. 21. As the coupling gets stronger, the Δ_1^2 and Δ_2^2 lines move downward/leftward, further away from the Δ_3^2 line, and the ratio ζ increases.

Now that we are convinced that the ϵ and η terms fully describe the M_s-dependent physics in our model at small M_s, we calculate ϵ and η, from diagrams like those in Fig. 22. After some calculation, the result is

$$\begin{aligned}\epsilon =& \frac{M_s^2}{4\pi^2\mu}\int_0^\Lambda dp\, p^2\Bigg\{\frac{1}{(p-\mu)^2}\tanh\left(\frac{p-\mu}{2T_c}\right) - \frac{1}{(p+\mu)^2}\tanh\left(\frac{p+\mu}{2T_c}\right) \\ &- \frac{\mu}{2T_c\, p(p-\mu)}\left[\cosh\left(\frac{p-\mu}{T_c}\right)\right]^{-2} - \frac{\mu}{2T_c\, p(p+\mu)}\left[\cosh\left(\frac{p+\mu}{T_c}\right)\right]^{-2}\Bigg\} \end{aligned} \tag{38}$$

$$\begin{aligned}\eta =& \frac{\mu_e}{2\pi^2}\int_0^\Lambda dp\, p^2\Bigg\{\frac{1}{(p-\mu)^2}\tanh\left(\frac{p-\mu}{2T_c}\right) - \frac{1}{(p+\mu)^2}\tanh\left(\frac{p+\mu}{2T_c}\right) \\ &- \frac{1}{2T_c(p-\mu)}\left[\cosh\left(\frac{p-\mu}{T_c}\right)\right]^{-2} + \frac{1}{2T_c(p+\mu)}\left[\cosh\left(\frac{p+\mu}{T_c}\right)\right]^{-2}\Bigg\} . \end{aligned} \tag{39}$$

In the weak-coupling limit, $T_c \ll \mu$ and the integrals are dominated by p within T_c of μ. In this limit, it is easy to check that $\zeta = \epsilon/\eta = M_s^2/2\mu\mu_e$, which yields $\zeta = 2$ since $\mu_e = M_s^2/4\mu$. At non-infinitesimal coupling, for example taking $\Delta_0 = 25$ MeV and reading the corresponding T_c from Fig. 1, we can evaluate ϵ and η. We find $\zeta = 2.55$ if we use $\mu_e = M_s^2/4\mu$, and if instead we obtain μ_e from our numerical results, we find $\zeta = 2.52$. Taking T_c and μ_e from our numerical results and evaluating ζ using (38,39) we find $\zeta = 2.52$, 2.65, 3.84 for $\Delta_0 = 25$, 40, 100 MeV respectively. From our numerical results, we have found $\zeta = 2.52$, 2.69, 3.87 at these values of Δ_0, extracting ζ from the ratio (36) as in (37). The agreement between these determinations is a confirmation of the accuracy of our numerical methods.

It is nice to see how quantitatively well the Ginzburg-Landau approximation describes the physics near T_c in our model, as we have demonstrated. Furthermore, the

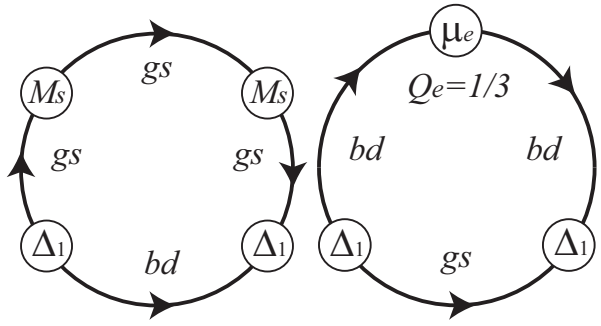

FIG. 22: Diagrams contributing to the ϵ and η terms in the Ginzburg Landau potential (32).

value of one of the two ratios of coefficients that we have investigated, $\beta_1/\beta_2 = 1$, is the same in our model and in QCD at asymptotic densities. And, the value of the other ratio $\zeta = \epsilon/\eta$ is comparable in our model to its value in QCD at asymptotic densities for $\Delta_0 = 25$ and 40 MeV, becoming significantly larger only for quite strong coupling, as at $\Delta_0 = 100$ MeV.

VII. IMPLICATIONS AND OPEN QUESTIONS

The phase diagrams shown in Figs. 1, 16 and 17 constitute the central results of this paper. They could be used in one of two different ways. If future theoretical advances constrain the μ-dependent values of Δ_0 and M_s more tightly than at present, these phase diagrams (and those that interpolate between them for other values of Δ_0) could be used to construct the phase diagram of nature. Or, if future astrophysical observations teach us that the phase diagram of nature must have certain features, for example must or must not include a certain phase, then the phase diagrams we have constructed could be used to draw inferences about the magnitudes of Δ_0 and M_s.

In thinking about the future phenomenological use of the phase diagrams that we have found, their complexity raises concerns. However, in most astrophysical contexts compact stars have temperatures much less than 1 MeV. At such low temperatures, which can be thought of as $T = 0$ in a QCD context, the phase diagrams are more manageable. We have the CFL phase at asymptotic densities, with the gCFL phase taking over at lower densities, when $\mu < M_s^2/2\Delta$. If Δ_0 lies at the large end of its estimated range 10 MeV $< \Delta_0 <$ 100 MeV, it seems likely that hadronic matter will take over from gCFL (or even from CFL) meaning that the complexities that we have found in our phase diagrams at larger M_s^2/μ will likely be superseded by the transition to the hadronic phase.

If Δ_0 lies at the lower end of its allowed range, then in Fig. 1 we find a straightforward transition to "unpaired" quark matter as the density is decreased further and M_s^2/μ increases beyond the gCFL window. If we extend our pairing ansatz, we will certainly find some pairing in this regime at sufficiently low temperature. For example, perhaps weak pairing between quarks with the same flavor plays a role [7, 41], or perhaps it is the crystalline color superconducting phase [37, 42] that takes over from gapless CFL at lower densities. Recent developments [42] make the crystalline color superconducting phase look like the most viable contender [6].

The one astrophysical context in which the full complexity of the phase diagrams that we have analyzed must be faced head-on is the physics of the proto-neutron star formed during a supernova, and in particular of the propagation of neutrinos therein. Phenomena encoded in the phase diagrams that we have analyzed could ultimately result in observable consequences in the time-of-arrival distribution of the neutrinos detected from a future supernova [27, 29, 43]. The phenomenological implications of the complexity of the phase diagrams (with many phase transition lines, the doubly critical point, the tricritical point and the insulator to metal transition as the CFL phase is heated) will have to be thought through in this context. The analytic treatment of the insulator to metal crossover and the Ginzburg-Landau analysis of the physics near T_c for small $M_s^2/\mu T_c$ that we have presented in Sections V and VI could prove valuable in this context.

Our analysis leaves many open avenues of investigation that must still be followed to their conclusions. The effects if gauge field fluctuations must be investigated, as must those of K^0-condensation in the gapless CFL phase. The effects of the 't Hooft interaction should be included, and the quark masses should be treated as dynamical condensates to be solved for, rather than as parameters. The pairing ansatz should be generalized, for example to allow for a comparison between the free energies of the gapless CFL and crystalline phases in three-flavor QCD.

Finally, the stability of the gapless CFL phase needs to be investigated further, along the lines of Ref. [44]. These authors find that the g2SC phase is unstable, as is the 2SC phase near the 2SC→g2SC transition. This instability could reflect the known instability of the g2SC phase with respect to a mixed phase of charged components [45], it could reflect an instability with respect to the crystalline color superconducting phase, or it could reflect the existence of some inhomogeneous phase yet to be discovered. We know that the gCFL phase is stable with respect to mixed phases, except perhaps at the largest values of M_s^2/μ where it is found in our phase diagrams [6, 46]. It seems likely that at these large values of M_s^2/μ the gCFL phase may anyway be superseded by the crystalline phase [6, 42]. This could be clarified either by a direct free energy comparison of these two phases, or by a stability analysis of the gCFL phase as in Ref. [44].

Acknowledgments

We acknowledge helpful conversations with M. Alford, J. Bowers, M. Forbes, T. Hatsuda, M. Huang, J. Kundu,

T. Schaefer, I. Shovkovy and M. Tachibana. C. K. and K. R. thank the Institute for Nuclear Theory in Seattle for its hospitality. K. F. is grateful to D. Rischke for hospitality at the University of Frankfurt during the completion of this work. K. F. was supported by Japan Society for the Promotion of Science for Young Scientists. This research was supported in part by the U.S. Department of Energy (D.O.E.) under cooperative research agreement #DF-FC02-94ER40818.

[1] For reviews, see K. Rajagopal and F. Wilczek, arXiv:hep-ph/0011333; M. G. Alford, Ann. Rev. Nucl. Part. Sci. **51**, 131 (2001) [arXiv:hep-ph/0102047]; G. Nardulli, Riv. Nuovo Cim. **25N3**, 1 (2002) [arXiv:hep-ph/0202037]; S. Reddy, Acta Phys. Polon. B **33**, 4101 (2002) [arXiv:nucl-th/0211045]; T. Schäfer, arXiv:hep-ph/0304281; M. Alford, arXiv:nucl-th/0312007.

[2] M. G. Alford, K. Rajagopal and F. Wilczek, Nucl. Phys. B **537**, 443 (1999) [arXiv:hep-ph/9804403].

[3] K. Iida and G. Baym, Phys. Rev. D **63**, 074018 (2001) [Erratum-ibid. D **66**, 059903 (2002)] [arXiv:hep-ph/0011229];

[4] M. Alford and K. Rajagopal, JHEP **0206**, 031 (2002) [arXiv:hep-ph/0204001].

[5] M. Alford, C. Kouvaris and K. Rajagopal, Phys. Rev. Lett. **92**, 222001 (2004) [arXiv:hep-ph/0311286].

[6] M. Alford, C. Kouvaris and K. Rajagopal, Phys. Rev. D., to appear, arXiv:hep-ph/0406137.

[7] A. Schmitt, Q. Wang and D. H. Rischke, Phys. Rev. D **66**, 114010 (2002) [arXiv:nucl-th/0209050].

[8] B. I. Halperin, T. C. Lubensky and S. k. Ma, Phys. Rev. Lett. **32**, 292 (1974).

[9] T. Matsuura, K. Iida, T. Hatsuda and G. Baym, Phys. Rev. D **69**, 074012 (2004) [arXiv:hep-ph/0312042].

[10] I. Giannakis, D. f. Hou, H. c. Ren and D. H. Rischke, arXiv:hep-ph/0406031.

[11] A. W. Steiner, S. Reddy and M. Prakash, Phys. Rev. D **66**, 094007 (2002) [arXiv:hep-ph/0205201].

[12] P. F. Bedaque and T. Schafer, Nucl. Phys. A **697**, 802 (2002) [arXiv:hep-ph/0105150]; D. B. Kaplan and S. Reddy, Phys. Rev. D **65**, 054042 (2002) [arXiv:hep-ph/0107265]; A. Kryjevski, D. B. Kaplan and T. Schafer, arXiv:hep-ph/0404290.

[13] A. Kryjevski and T. Schaefer, arXiv:hep-ph/0407329; A. Kryjevski and D. Yamada, arXiv:hep-ph/0407350.

[14] W. V. Liu, F. Wilczek and P. Zoller, arXiv:cond-mat/0404478.

[15] S. B. Rüster, I. A. Shovkovy and D. H. Rischke, arXiv:hep-ph/0405170.

[16] K. Iida, T. Matsuura, M. Tachibana and T. Hatsuda, arXiv:hep-ph/0312363.

[17] K. Iida and G. Baym, Phys. Rev. D **66**, 014015 (2002) [arXiv:hep-ph/0204124].

[18] M. G. Alford, J. Berges and K. Rajagopal, Nucl. Phys. B **558**, 219 (1999) [arXiv:hep-ph/9903502].

[19] M. G. Alford, J. Berges and K. Rajagopal, Nucl. Phys. B **571**, 269 (2000) [arXiv:hep-ph/9910254].

[20] D. K. Hong, Nucl. Phys. B **582**, 451 (2000) [arXiv:hep-ph/9905523]; N. J. Evans, J. Hormuzdiar, S. D. H. Hsu and M. Schwetz, Nucl. Phys. B **581**, 391 (2000) [arXiv:hep-ph/9910313].

[21] R. Rapp, T. Schafer, E. V. Shuryak and M. Velkovsky, Annals Phys. **280**, 35 (2000) [arXiv:hep-ph/9904353].

[22] T. Schafer, Nucl. Phys. B **575**, 269 (2000) [arXiv:hep-ph/9909574].

[23] C. Manuel and M. H. G. Tytgat, Phys. Lett. B **479**, 190 (2000) [arXiv:hep-ph/0001095].

[24] T. Schafer, Phys. Rev. D **65**, 094033 (2002) [arXiv:hep-ph/0201189].

[25] D. T. Son and M. A. Stephanov, Phys. Rev. D **61**, 074012 (2000) [arXiv:hep-ph/9910491]; Phys. Rev. D **62**, 059902 (2000) [arXiv:hep-ph/0004095].

[26] D. K. Hong, T. Lee and D. P. Min, Phys. Lett. B **477**, 137 (2000) [arXiv:hep-ph/9912531]; S. R. Beane, P. F. Bedaque and M. J. Savage, Phys. Lett. B **483**, 131 (2000) [arXiv:hep-ph/0002209]; T. Schafer, Phys. Rev. D **65**, 074006 (2002) [arXiv:hep-ph/0109052].

[27] S. Reddy, M. Sadzikowski and M. Tachibana, Nucl. Phys. A **714**, 337 (2003) [arXiv:nucl-th/0203011].

[28] P. Jaikumar, M. Prakash and T. Schafer, Phys. Rev. D **66**, 063003 (2002) [arXiv:astro-ph/0203088]; I. A. Shovkovy and P. J. Ellis, Phys. Rev. C **66**, 015802 (2002) [arXiv:hep-ph/0204132].

[29] J. Kundu and S. Reddy, arXiv:nucl-th/0405055.

[30] P. Amore, M. C. Birse, J. A. McGovern and N. R. Walet, Phys. Rev. D **65**, 074005 (2002) [arXiv:hep-ph/0110267].

[31] A. Gerhold and A. Rebhan, Phys. Rev. D **68**, 011502 (2003) [arXiv:hep-ph/0305108]; A. Kryjevski, Phys. Rev. D **68**, 074008 (2003) [arXiv:hep-ph/0305173]; D. D. Dietrich and D. H. Rischke, Prog. Part. Nucl. Phys. **53**, 305 (2004) [arXiv:nucl-th/0312044].

[32] K. Rajagopal and F. Wilczek, Phys. Rev. Lett. **86**, 3492 (2001) [arXiv:hep-ph/0012039].

[33] J. M. Cornwall, R. Jackiw and E. Tomboulis, Phys. Rev. D **10**, 2428 (1974).

[34] M. Buballa and M. Oertel, Nucl. Phys. A **703**, 770 (2002) [arXiv:hep-ph/0109095]; F. Neumann, M. Buballa and M. Oertel, Nucl. Phys. A **714**, 481 (2003) [arXiv:hep-ph/0210078].

[35] I. Shovkovy and M. Huang, Phys. Lett. B **564**, 205 (2003) [arXiv:hep-ph/0302142]; M. Huang and I. Shovkovy, arXiv:hep-ph/0307273.

[36] E. Gubankova, W. V. Liu and F. Wilczek, Phys. Rev. Lett. **91**, 032001 (2003).

[37] P. Fulde and R. A. Ferrell, Phys. Rev. **135**, A550 (1964); S. Takada and T. Izuyama, Prog. Theor. Phys. **41**, 635 (1969); M. G. Alford, J. A. Bowers and K. Rajagopal, Phys. Rev. D **63**, 074016 (2001) [arXiv:hep-ph/0008208]; J. .A. Bowers, J. Kundu, K. Rajagopal and E. Shuster, Phys. Ref. D **64**, 014024 (2001) [arXiv:hep-ph/0101067]; J. Kundu and K. Rajagopal, Phys. Rev. D **65**, 094022 (2002) [arXiv:hep-ph/0112206]; J. A. Bowers and K. Rajagopal, Phys. Rev. D **66**, 065002 (2002) [arXiv:hep-ph/0204079]; R. Casalbuoni and G. Nardulli, Rev. Mod. Phys. **263**, 320 (2004) [arXiv:hep-ph/0305069].

[38] G. Sarma, J. Phys. Chem. Solids **24**, 1029 (1963).

[39] M. G. Alford, J. Berges and K. Rajagopal, Phys. Rev. Lett. **84**, 598 (2000) [arXiv:hep-ph/9908235].
[40] A. Sedrakian and U. Lombardo, Phys. Rev. Lett. **84**, 602 (2000) [arXiv:nucl-th/9907076].
[41] M. Iwasaki and T. Iwado, Phys. Lett. B **350**, 163 (1995); M. G. Alford, K. Rajagopal and F. Wilczek, Phys. Lett. B **422**, 247 (1998) [arXiv:hep-ph/9711395]; T. Schafer, Phys. Rev. D **62**, 094007 (2000) [arXiv:hep-ph/0006034]; M. Buballa, J. Hosek and M. Oertel, Phys. Rev. Lett. **90**, 182002 (2003) [arXiv:hep-ph/0204275]; M. G. Alford, J. A. Bowers, J. M. Cheyne and G. A. Cowan, Phys. Rev. D **67**, 054018 (2003) [arXiv:hep-ph/0210106]; A. Schmitt, arXiv:nucl-th/0405076.
[42] R. Casalbuoni, M. Ciminale, M. Mannarelli, G. Nardulli, M. Ruggieri and R. Gatto, arXiv:hep-ph/0404090.
[43] G. W. Carter and S. Reddy, Phys. Rev. D **62**, 103002 (2000) [arXiv:hep-ph/0005228].
[44] M. Huang and I. A. Shovkovy, arXiv:hep-ph/0407049.
[45] P. F. Bedaque, H. Caldas and G. Rupak, Phys. Rev. Lett. **91**, 247002 (2003) [arXiv:cond-mat/0306694]; M. M. Forbes, E. Gubankova, W. V. Liu and F. Wilczek, arXiv:hep-ph/0405059; S. Reddy and G. Rupak, arXiv:nucl-th/0405054.
[46] M. Alford, C. Kouvaris and K. Rajagopal, arXiv:hep-ph/0407257.
[47] We have learned from them in private communications that the authors of Ref. [15] now find an ordering of phase transitions in agreement with our results and the Ginzburg-Landau analysis.